Bioactive Materials 25 (2023) 766–782

Contents lists available at ScienceDirect

Bioactive Materials

journal homepage: www.keaipublishing.com/en/journals/bioactive-materials

Autologous exosome facilitates load and target delivery of bioactive peptides to repair spinal cord injury

Ning Ran [a,b,1], Wenxiang Li [b,a,1], Renjie Zhang [b,a], Caorui Lin [d], Jianping Zhang [c], Zhijian Wei [a,b,c], Zonghao Li [b,a], Zhongze Yuan [b,a], Min Wang [f], Baoyou Fan [c], Wenyuan Shen [c], Xueying Li [a], Hengxing Zhou [a,b,c], Xue Yao [a,c], Xiaohong Kong [a,b,e,**], Shiqing Feng [a,b,c,*]

[a] Orthopedic Research Center of Shandong University &Advanced Medical Research Institute, Cheeloo College of Medicine, Shandong University, Jinan, Shandong, China
[b] Department of Orthopedics, Qilu Hospital of Shandong University, Jinan, Shandong, China
[c] Tianjin Key Laboratory of Spine and Spinal Cord, National Spinal Cord Injury International Cooperation Base, Department of Orthopedics, Tianjin Medical University General Hospital, Tianjin, China
[d] Fujian Key Laboratory of Laboratory Medicine, The First Affiliated Hospital, Fujian Medical University, Fuzhou, Fujian, China
[e] Laboratory of Medical Molecular Virology, School of Medicine, Nankai University, Tianjin, China
[f] Tianjin Key Laboratory of Lung Cancer Metastasis and Tumor Microenvironment, Tianjin Lung Cancer Institute, Tianjin Medical University General Hospital, Tianjin, China

ARTICLE INFO

Keywords:
Spinal cord injury
Targeted repair
Autologous plasma exosome
Drug loading
Axon regeneration

ABSTRACT

Spinal cord injury (SCI) causes motor, sensory and automatic impairment due to rarely axon regeneration. Developing effective treatment for SCI in the clinic is extremely challenging because of the restrictive axonal regenerative ability and disconnection of neural elements after injury, as well as the limited systemic drug delivery efficiency caused by blood spinal cord barrier. To develop an effective non-invasive treatment strategy for SCI in clinic, we generated an autologous plasma exosome (AP-EXO) based biological scaffold where AP-EXO was loaded with neuron targeting peptide (RVG) and growth-facilitating peptides (ILP and ISP). This scaffold can be targeted delivered to neurons in the injured area and elicit robust axon regrowth across the lesion core to the levels over 30-fold greater than naïve treatment, thus reestablish the intraspinal circuits and promote motor functional recovery after spinal cord injury in mice. More importantly, in *ex vivo*, human plasma exosomes (HP-EXO) loaded with combinatory peptides of RVG, ILP and ISP showed safety and no liver and kidney toxicity in the application to nude SCI mice. Combining the efficacy and safety, the AP-EXO-based personalized treatment confers functional recovery after SCI and showed immense promising in biomedical applications in treating SCI. It is helpful to expand the application of combinatory peptides and human plasma derived autologous exosomes in promoting regeneration and recovery upon SCI treatment.

1. Introduction

Spinal cord injury (SCI) causes irreversible damage and permanent functional loss of motor, sensory and autonomic (sexual, urinary, cardiovascular and intestinal) and spontaneous recovery is limited [1,2] as well. Such loss of function is due to the neuron death and the failure of neuron regeneration. To date, there is no cure available for SCI in clinic, apart from methylprednisolone for suppressing inflammation at early stage of injury [3]. Though many drugs or composite methods have been used in protecting neuronal death and promoting axonal regeneration [4–6]. The crucial obstacles restricting axonal sprouting and limiting neuroplasticity after SCI include cellular and myelin debris

Abbreviations: SCI, Spinal Cord Injury.

Peer review under responsibility of KeAi Communications Co., Ltd.

* Corresponding author. Orthopedic Research Center of Shandong University &Advanced Medical Research Institute, Cheeloo College of Medicine, Shandong University, Jinan, Shandong, China.
** Corresponding author. Orthopedic Research Center of Shandong University &Advanced Medical Research Institute, Cheeloo College of Medicine, Shandong University, Jinan, Shandong, China.
E-mail addresses: kongxh@sdu.edu.cn (X. Kong), shiqingfeng@sdu.edu.cn (S. Feng).

[1] These authors contribute equally to the work.

https://doi.org/10.1016/j.bioactmat.2022.07.002
Received 4 May 2022; Received in revised form 3 July 2022; Accepted 3 July 2022
Available online 22 July 2022

inflammatory response, as well as glia scar, where reactive astrocytes and extracellular matrix contents of chondroitin sulfate proteoglycans (CSPGs) are the major components [7–9]. To this end, relieve the inhibition of CSPGs and reactivate the intrinsic neuronal growth ability have been explored [10,11]. Inhibition of the binding of CSPGs to neuronal receptors such as leukocyte common antigen-related (LAR) [12] and protein tyrosine phosphatase σ (PTPσ) [10,11] with peptide ILP or ISP have shown to alleviate the pathological progression and led to robust axon regeneration and functional recovery after SCI in mice model. Despite these promising findings, the inability of ILP or ISP to effectively inhibit the binding of neurons to CSPGs can be largely attributed to the poor permeability of blood spinal cord barrier (BSCB), serum stability and low bioavailability as injection of cell penetrating peptides (CPPs) conjugated ILP or ISP resulted in functional improvements after spinal cord injury. Therefore, a strategy that addresses both issues may increase the efficacy of the ILP and ISP.

Efficient delivery of functional cargos into the injured spinal cord is recognized as one of the biggest challenges, because most of the cargos are hard to cross the BSCB and reach the injured site. Recent years, increasing research efforts of nanovector-mediated drug delivery have been made in selectively targeting to specific cells and improving the delivery efficacy [13]. Alternatively, as nanovesicles secreted from various cells, exosomes have come into being as vital candidates for drug delivery owing to their low immunogenicity [14], successfully crossing the BSCB [13] and evasion from phagocytosis [15]. What's more, exosomes from different cell sources, especially stem cells [16,17] have been tested in SCI repair by modulating autophagy, neuroprotection, angiogenesis and inflammation, eventually leading to glial scar reduction and functional recovery. However, limited production of exosomes and lack of site targeting may cause varying therapeutic responses. Cell-free culture (such as plasma) derived exosomes offer interesting alternatives and access to potentially large amounts of exosomes [18,19]. In this study, we use exosomes from autologous plasma (AP-EXO) as functional cargo-carriers which are free of triggering the immune response, and loaded with growth facilitating peptides (ILP and ISP) and targeting moieties (RVG) via CP05, a peptide which have been demonstrated efficiently in exosome's surface modification [20] to generate an AP-EXO-based multi-functional bioactive delivery system. We hypothesized that anchoring the multi-functional peptide on the surface can improve the targeting specificity, stability and consequently efficacy of bioactive peptide.

Here, we report the AP-EXO-based biological scaffolds for promoting robust axon regeneration, sustained and localized release of AP-EXO significantly enhanced functional recovery after SCI. Such a functional recovery is achieved in three ways: i) reducing the lesion size by inhibiting inflammatory response, ii) stimulating robust axon regrowth through astrocyte borders and across the lesion core to levels over 30-fold greater than naïve treatment, iii) promoting new intraspinal circuit formation crossing the lesion area and causing motor function recovery after injury. This study demonstrates a novel non-invasive biological repair strategy with a peptide-loaded exosome preparation that could augment motor functional recovery and offers some important insights into the clinical translation of exosomes loaded with three bioactive peptides in treating SCI.

2. Results

2.1. Design and evaluation of neuron-targeting- and growth-facilitating-peptide-modified AP-EXO promotes axon elongation in vitro

As our previous studies have demonstrated that exosomes are efficient delivery vehicles and can be loaded with various cargos such as peptides on the surface via a linker peptide CP05. Here, we generated neuron-targeting and growth-facilitating peptide-loaded AP-EXO and

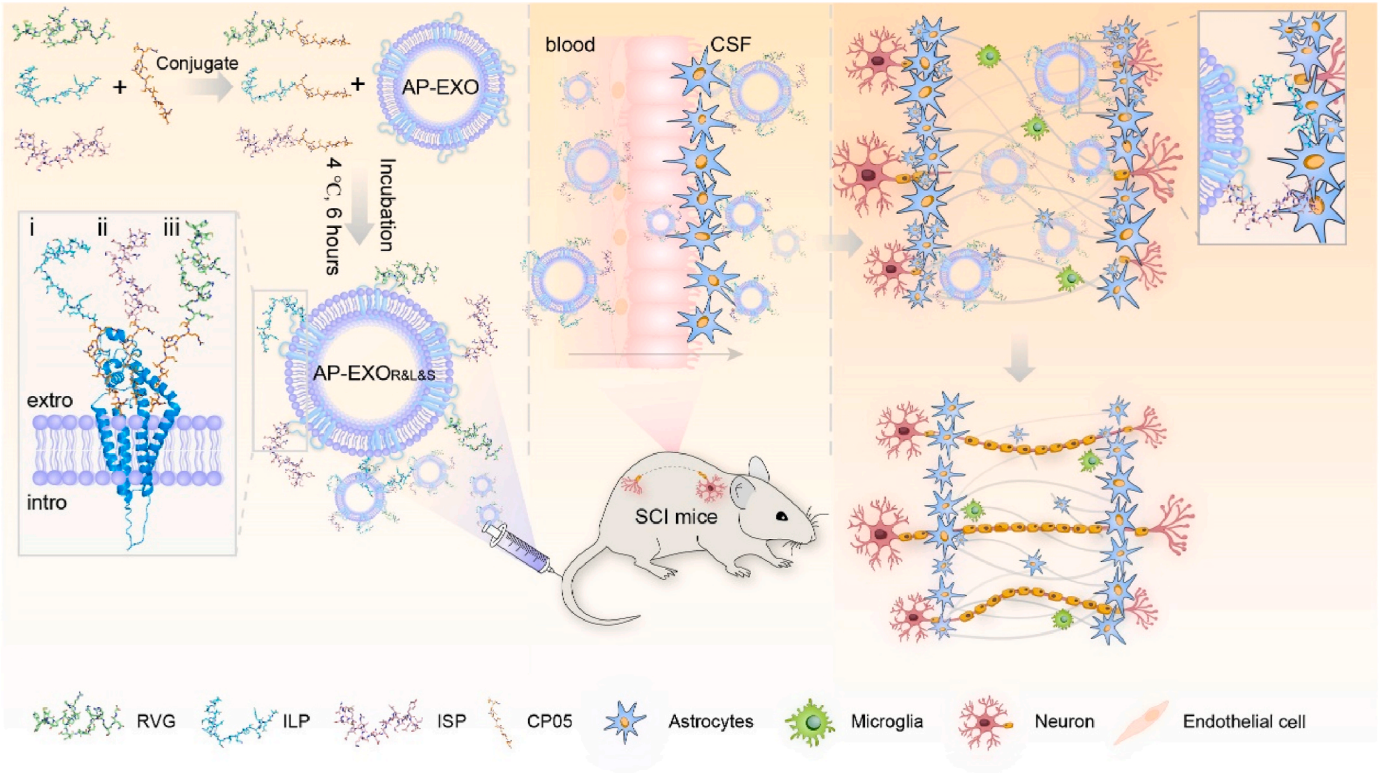

Fig. 1. Graphic abstract illustrating the construction of engineered AP-EXO target delivery to repair spinal cord injury. AP-EXO was simultaneously surface loaded with neuron targeting peptide RVG and growth-promoting peptide (ILP and ISP) via CP05 to generate AP-EXO$_{R\&L\&S}$. This AP-EXO-based biological scaffold enabled targeting delivery of AP-EXO$_{R\&L\&S}$ crossing the blood-spinal cord barriers into the neurons of the injured spinal cord and boosted robust axon regeneration thus promoting motor functional recovery after spinal cord injury.

detected their function in promoting axon elongation *in vivo* (Fig. 1). To confirm whether multi-bioactive moieties could be anchored on AP-EXO, we firstly determined the CD63 expression and measured the number of CP05 linked to AP-EXO by using immunogold electron microscope. Not surprisingly, AP-EXO presented high CD63 expression (Supplementary Fig. 1a) and more than 10 gold-labeled CP05 peptides were detectable on the AP-EXO surface (Supplementary Fig. 1b). Here, we used different fluorescence markers to label the three bioactive peptides (Cy5.5-labeled RVG-CP05, FAM-labeled ILP-CP05 and MCA (7-Methoxycoumarin-4-acetic)-labeled ISP-CP05) and generated the RVG-CP05, ILP-CP05 and ISP-CP05 modified AP-EXO (AP-EXO$_{R\&L\&S}$). On one side, the peptides were distinguished by different markers; and on the other, we tried to distinguish the repair degree after SCI by using different markers and modification. In particularly, ILP can bind to LAR (latent antigen related) and promote axon growth [21], and ISP can bind to PTPσ and relieve CSPGs-mediated inhibition. When single peptide or three peptides combinatory incubated with AP-EXO, as expected, each of the three peptides showed a binding efficiency of approximately 90% (Supplementary Fig. 1c), and over 76% of AP-EXO could be decorated by three combinatory peptides (Fig. 2a), which may due to the competition to some degree among the three peptides. Furthermore, we detected the morphology and size of AP-EXO or AP-EXO$_{R\&L\&S}$, both of them presented the typical sauce shaped morphology and within the normal size range of exosomes, indicating that triple peptide modification doesn't alter the morphology and size of the original AP-EXO (Fig. 2b and c). To visualize the anchoring of the three peptides to AP-EXO directly, designated fluorescence marker labeled AP-EXO$_{R\&L\&S}$ was incubated with polystyrene beads and then fluorescence microscopic image was taken to trace the exosomes, remarkable fluorescence of the colocalization of AP-EXO with three peptides was observed in AP-EXO$_{R\&L\&S}$ group (Fig. 2d). Overall, these results demonstrated that AP-EXO were anchored efficiently by the three bioactive peptides.

To determine whether AP-EXO could facilitate cellular uptake of the three peptides, AP-EXO$_{R\&L\&S}$ was cultured with HT22 (neuronal cell line) and primary cortical neurons, and observed by fluorescence imaging, it revealed that the bulk of three peptides can be integrated into cells and they were colocalized in the cytoplasm (Supplementary Fig. 1d). Furthermore, we employed axonal guidance spot assays to evaluate whether AP-EXO$_{R\&L\&S}$ could promote axon elongation towards CSPG-spot barrier. Consistent with a previous study [22], CSPG-mediated inhibition of primary cortical neurocytes appeared to be dose-dependent and 2.5 μg/ml was chosen as the optimal concentration in our study (Supplementary Fig. 1e). Strikingly, AP-EXO$_{R\&L\&S}$ treatment allowed ≥80% of cortical neurons to extend axons through CSPG barriers with ≥3 axons per cell, while the peptide RVG-CP05, RVG-ILP and RVG-ISP alone failed to show the similar effect of combinatory peptides of AP-EXO$_{R\&L\&S}$ (Fig. 2e–g). Additionally, AP-EXO$_{R\&L\&S}$ boosted axon elongation and increased the branches of cortical neurons cultured in CSPG medium (Fig. 2h–j). Taken together, these data provide substantial evidence that AP-EXO$_{R\&L\&S}$ rescues CSPG-mediated inhibition of neurons *in vitro*.

2.2. AP-EXO$_{R\&L\&S}$ targets the injured spinal cord in SCI mice

To determine the targeting property of AP-EXO$_{R\&L\&S}$ to spinal cord, especially in neurons around the lesion site after spinal cord injury. Firstly, we validated the ability of RVG targeting the spinal cord and found a substantial amount of Cy5.5-RVG in spinal cord (Supplementary Fig. 2a). We have reported targeting moiety-decorated exosomes showed specific organic tropism [20]. Since neuron-specific rabies viral glycoprotein (RVG) is known to bind the p75 neurotrophin receptor (p75NTR) and accelerate its axonal retrograde transport [23]. It is intriguing to investigate whether RVG-CP05 facilitate AP-EXO homing to the spinal cord, especially in injured spinal cord where AP-EXO localized in the injury site. Firstly, we intravenously injected AP-EXO$_{R\&L\&S}$ in the wild type C57BL/6 mice (PKH26 labeled AP-EXO 30 μg incubated with the same amount of rhodamine-labeled ISP-CP05, FAM-labeled ILP-CP05 and Alexa Fluor 405-labeled RVG-CP05) to detect the homing ability of AP-EXO in wild type C57BL/6 mice and we found that RVG could facilitate AP-EXO$_{R\&L\&S}$ targeted aggregation in the brain and spinal cord (Supplementary Fig. 2b). Here, the dose of 30 μg was validated in our previous studies [20]. Furthermore, we used contusive SCI mice model, which could simulate the pathology of patient suffered from spinal cord injury in clinic, to test the homing ability of AP-EXO$_{R\&L\&S}$ into SCI mice spinal cord. Firstly, we made the sagittal section and coronal section of the injured spinal cord and stained with NF200 to verify the homogeneity of our mice mode (Supplementary Fig. 2d). AP-EXO$_{R\&L\&S}$ (DiR labeled AP-EXO (30 μg)) loaded with the same amount of RVG-CP05, ILP-CP05 and ISP-CP05 was intravenously injected into contusive SCI mice (Fig. 3a), As expected, *ex vivo* imaging revealed that fluorescence intensity was significantly increased in mice injected with AP-EXO$_{R\&L\&S}$ compared to those injected with AP-EXO (Fig. 3b and c) at 2 h post injection. We further confirmed that DiR labeled AP-EXO distributed exclusively in the area of the injured spinal cord in the AP-EXO$_{R\&L\&S}$-treated mice (Fig. 3d and e). In particular, the majority of AP-EXOs were colocalized with neurons, while only a small part of AP-EXOs were colocalized with astrocytes or microglia at injured sites in AP-EXO$_{R\&L\&S}$-injected mice (Fig. 3f, Supplementary Fig. 2c). To understand the dynamic time of AP-EXO$_{R\&L\&S}$ in the injury spinal cord, we examined the fluorescence of DiR labeled AP-EXO in the spinal cord after single injection of AP-EXO$_{R\&L\&S}$ at a dose of 30 μg (DiR-labeled AP-EXO 30 μg incubated with the same of amount of rhodamine-labeled ISP-CP05, FAM-labeled ILP-CP05 and Alexa Fluor 405-labeled RVG-CP05), the results showed approximately 50% of AP-EXO$_{R\&L\&S}$ could be detected in the spinal cord at day 1 after injection, and more importantly, approximately 16% AP-EXO$_{R\&L\&S}$ was detectable at day 7 after injection, compared to AP-EXO$_{R\&L\&S}$'s aggregation at the time point of 2 h post injection. (Fig. 3g and h). We also detected the binding of three peptides to AP-EXO in the injury site at the time point of 2 h, 1 day, 3 days and 7 days after administration. Strikingly, a weaker colocalization of three peptides to AP-EXO was still detected 7 days after injection (Fig. 3i and j). Colocalization assessment revealed a peak binding of the peptides to AP-EXO at 2 h with a descent from 1 day to 7 days after injection (Fig. 3j), suggesting that anchored peptides to the AP-EXO were slowly released in the injured spinal cord. Next, we used neurocyte-astrocyte co-culture cell system [22] to confirm that AP-EXO$_{R\&L\&S}$ distributed in Tuj-1 positive neurocytes rather than in ALDH1L1-labeled astrocytes. In contrast, the majority of AP-EXO (> 60%) was endocytosed by astrocytes (Fig. 3k-l). Overall, these findings implicated that AP-EXO$_{R\&L\&S}$ enables its homing competency to SCI injury sites where multifunctional peptide-loaded AP-EXO exerted their potential effect on SCI repair by directly targeting the lesion sites.

2.3. AP-EXO$_{R\&L\&S}$ enables axon regeneration and motor function recovery after spinal cord contusion in SCI mice

We wondered whether multi-bioactive peptides-loaded AP-EXO could promote axon regeneration and functional recovery after SCI *in vivo*. Firstly, we examined the therapeutic effect of AP-EXO$_{R\&L\&S}$ in contused SCI mice model. Age-matched adult mice were subjected to spinal cord contusion and received direct intravenous injection of AP-EXO, AP-EXO$_{RVG}$, AP-EXO$_{ILP}$, AP-EXO$_{ISP}$ or AP-EXO$_{R\&L\&S}$ starting at day 1 after injury at a dose of 1 mg/kg per week for 5 weeks, an administration strategy optimized by previous studies [24–26] and then mice received an injection of biotinylated dextran amine 10000 (BDA) into the bilateral sensorimotor cortex immediately afterward (Fig. 4a). Systemic administration of AP-EXO$_{R\&L\&S}$ induced dramatically reduction of GFAP-positive in sequential sagittal section, moreover, neurons were mainly redistributed in the injured area in the corresponding sagittal section of AP-EXO- and AP-EXO$_{R\&L\&S}$-injected groups (Fig. 4b and c). Notably, compared with the PBS-injected SCI group, more than

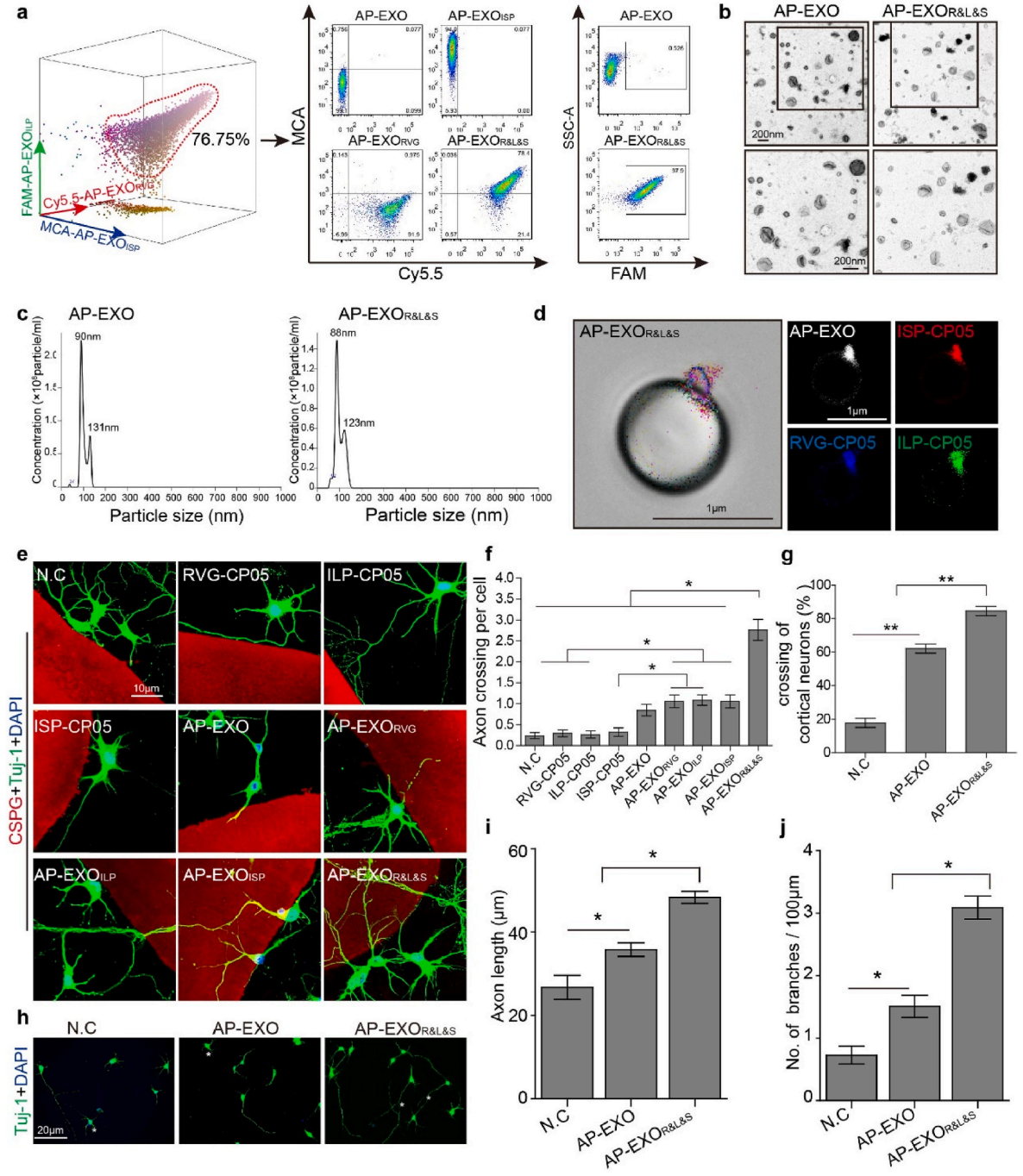

Fig. 2. Generation of AP-EXO$_{R\&L\&S}$ and evaluation of their ability to promote axon elongation *in vitro*. (a) Flow cytometry for measuring the loading efficiency of RVG-CP05, ILP-CP05 and ISP-CP05 to AP-EXO. Cy5.5 labeled RVG-CP05 (10 μg), FAM labeled ILP-CP05 (10 μg) and MCA labeled ISP-CP05 (10 μg) were co-incubated with AP-EXO (10 μg) together at 4 °C for 6 h, the non-specific binding peptides were removed by ultracentrifugation. AP-EXO$_{RVG}$ indicated AP-EXO loaded with RVG-CP05, AP-EXO$_{ISP}$ indicated AP-EXO decorated by ISP-CP05, AP-EXO$_{ILP}$ indicated AP-EXO decorated by ILP-CP05. AP-EXO$_{R\&L\&S}$ represents AP-EXO simultaneously painted by RVG-CP05, ILP-CP05 and ISP-CP05. Left 3D images show the simultaneously binding efficiency of three peptides on AP-EXO, right 2D images show the analysis process. Cy5.5 as the indicator of horizontal axis and MCA as the indicator of vertical axis for those four exosomes showed in the middle panel of Fig. 2a, and also FAM as the indicator of the horizontal axis in the right panel of Fig. 2a. **(b)** Representative TEM images of AP-EXO and AP-EXO$_{R\&L\&S}$. Scale bar: 200 nm. TEM, Transmission electron microscope. **(c)** Size distribution of AP-EXO and AP-EXO$_{R\&L\&S}$. **(d)** Representative confocal images showing binding and colocalization of rhodamine-labeled ISP-CP05, FAM-labeled ILP-CP05 and Alexa Fluor 405-labeled RVG-CP05 with DiR-labeled AP-EXO on polystyrene beads. Scale bar: 1 μm. **(e–g)** Axonal guidance spot assays to evaluate the ability of AP-EXO$_{R\&L\&S}$ in promoting axonal elongation toward the CSPG-spot barrier. **e**, representative images of primary cortical neurons cross the CSPG-spot barrier after AP-EXO$_{R\&L\&S}$ incubation. Scale bar:10 μm. **f**, quantitative analysis of axons crossing the CSPG barrier per primary cortical neuron (n = 34, $*p < 0.05$, one way ANOVA on ranks post Dunn's Method). **g**, the comparison of cortical neurons crossing the CSPG barrier across 3 groups (n = 4, $**p < 0.001$, one-way ANOVA post Student-Newman-Keuls test). **(h–j)** Axon elongation of primary cortical neurons cultured in CSPG medium. **h**, representative images of axon length and branches (asterisk) number after AP-EXO$_{R\&L\&S}$ treatment. Scale bar: 20 μm. **i**, quantification of axon length (NC: n = 51, AP-EXO: n = 95, AP-EXO$_{R\&L\&S}$: n = 135. $*p < 0.05$, one way ANOVA on ranks post Dunn's Method). **j,** quantification of branches number shown in (h) (NC: n = 48, AP-EXO: n = 57, AP-EXO$_{R\&L\&S}$: n = 69. $*p < 0.05$, one way ANOVA on ranks post Dunn's Method).

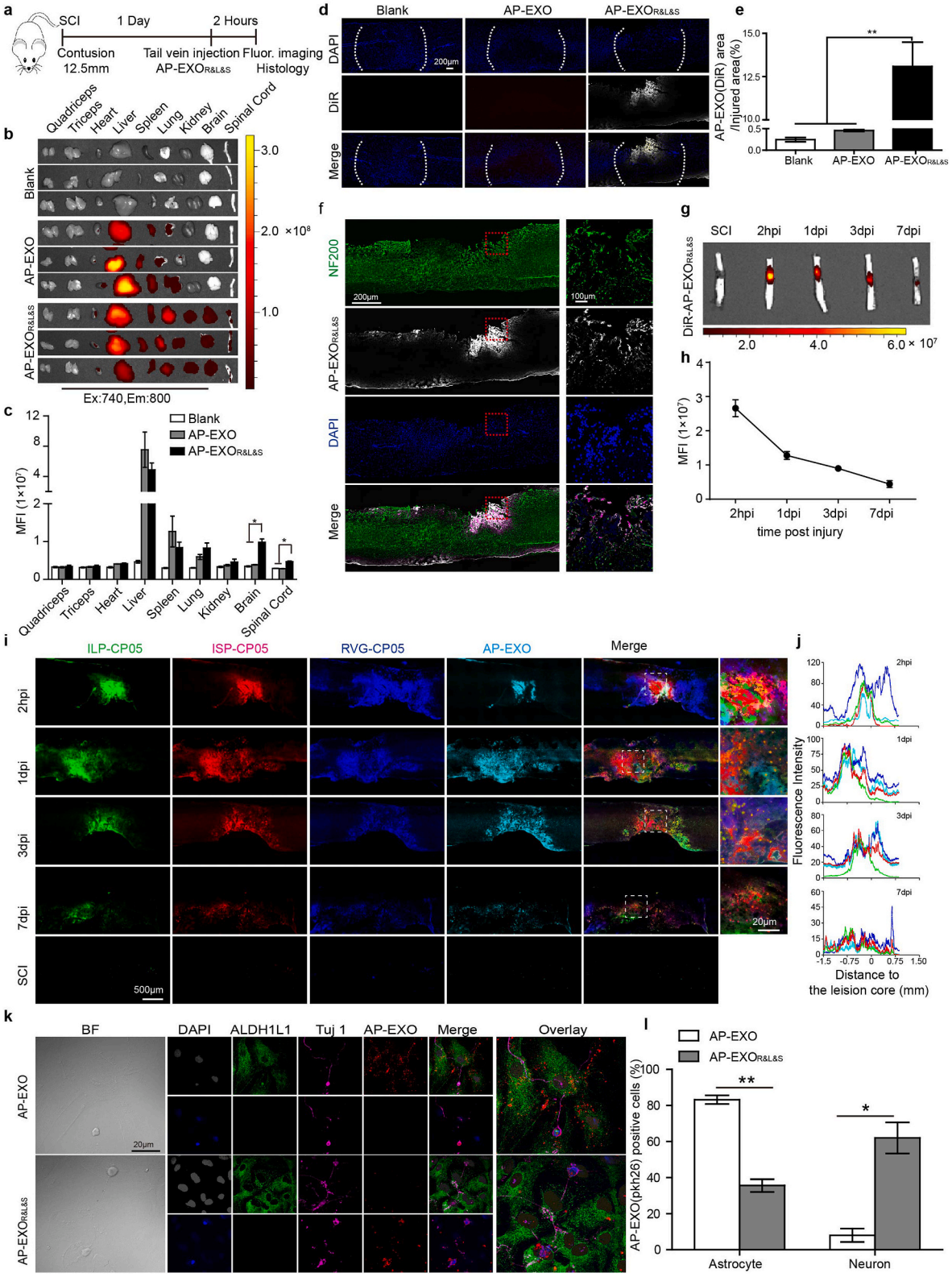

(caption on next page)

Fig. 3. Distribution of AP-EXO$_{R\&L\&S}$ *in vivo* and *in vitro*. (a) Timeline of surgical interventions for experiments presented in (a–f) and Supplementary Figs. 2b–c. Spinal cord contused C57BL/6 mice received a single intravenous injection of DiR-labeled AP-EXO or AP-EXO$_{R\&L\&S}$ (30 μg). After 2 h, the mice were sacrificed and the fluorescence of different tissues was imaged. Blank designated as the mice injected with PBS. AP-EXO designated as the mice injected with DiR-labeled AP-EXO. AP-EXO$_{R\&L\&S}$ designated as the mice injected with RVG-CP05, ILP-CP05 and ISP-CP05 loaded AP-EXO. **(b)** Distribution of fluorescence intensity in body-wide tissues. **(c)** Quantitative analysis of fluorescence intensity in body-wide tissues. (n = 3, $*p < 0.05$, Brain, one-way ANOVA on ranks post Tukey Test. Spinal cord, one-way ANOVA post Student-Newman-Keuls test). **(d)** Representative images of DiR-labeled AP-EXO in injured region after AP-EXO or AP-EXO$_{R\&L\&S}$ injected. Scale bar: 200 μm. **(e)** Quantitative comparison of the ratio of the DiR-labeled AP-EXO distributed area to injured area across 3 groups. (n = 3, $**p < 0.001$, one-way ANOVA post Student-Newman-Keuls test). **(f)** Representative images showing the colocalization of DiR-labeled AP-EXO with NF200-labeled neurons. Scale bar: 200 μm, inset: 100 μm. **(g–j)** Spinal cord contused C57BL/6 mice received a single intravenous injection of AP-EXO$_{R\&L\&S}$ (DiR-labeled AP-EXO 30 μg incubated with the same amount of rhodamine-labeled ISP-CP05, FAM-labeled ILP-CP05 and Alexa Fluor 405-labeled RVG-CP05) at determined time point. The mice were sacrificed at specified time point of 2 h, 1 d, 3 d, 7 d post injection and the fluorescence of different tissues was imaged. **g,** distribution for fluorescence intensity of AP-EXO in the injured spinal cord. **h,** quantitative analysis of fluorescence intensity at different time-points. Scale bar: 500 μm, inset: 100 μm. **i,** representative images for ISP-CP05, ILP-CP05, RVG-CP05 and AP-EXO localization in the injury sites. **j,** quantitative analysis of colocalization of ISP-CP05, ILP-CP05 and RVG-CP05 to AP-EXO. **(k)** Representative images showing the colocalization of pkh-26 labeled AP-EXO with ALDH1L1-positive primary astrocytes and Tuj 1- positive primary neurons after incubated with AP-EXO or AP-EXO$_{R\&L\&S}$ *in vitro*. Scale bar: 20 μm. **(l)** Quantitative comparison of AP-EXO (pkh26) positive astrocytes and neurons in 2 groups of AP-EXO or AP-EXO$_{R\&L\&S}$. (n = 5, $*p < 0.05$, $**p < 0.001$, two tailed *t*-test). Representative images of Fig. 2d and f and Supplementary Fig. 2c were from the same tissue.

half of the GFAP-positive areas were reduced in size in the AP-EXO- and AP-EXO$_{R\&L\&S}$-treated groups, suggesting AP-EXO also bearing therapeutic potency for modulating the microenvironment in the injured area [26]. Since the peptide ISP has been proven to enable the sprouting of serotonergic (5-HT positive) fibers below the level of lesion sites [11], we stained and analyzed these axons in sagittal spinal cord sections of the injury center or in transverse sections at the L1 level (Fig. 4d–g). PBS-treated SCI mice revealed a sprouting of 5-HT-positive axons across a distance of less than 2 mm, in comparing with the controls, remarkably, AP-EXO$_{R\&L\&S}$-treated mice showed more and longer-distance elongation of serotonergic fibers with ≥15% of axons across a distance of 5 mm (Fig. 4d and e). A sprouting of 5-HT-positive axons at L1 level was observed, especially in the raphe-spinal tract (Fig. 4f and g), which is reported relevant for locomotor recovery [27]. Interestingly, the terminal bulbs of the sprouted serotonergic fibers got in touch with membrane-bound ChAT (choline acetyltransferase) and coincided with synaptic vesicles (identified with the presynaptic marker synaptophysin, Syn1) (Supplementary Fig. 3a). We speculated that the sprouted serotonergic fibers, especially those were in touch with synaptic vesicles may account for the locomotor function recovery of spinal-cord-injured mice. Furthermore, we wondered whether AP-EXO$_{R\&L\&S}$ could enhance corticospinal tract (CST) regeneration or not? As receptors of the peptides ILP and ISP, LAR and PTPσ are widely expressed in different populations of neurons in brain and spinal cord [12], and could be co-stained with BDA positive neurons and 5-HT positive neurons (Supplementary Fig. 3b). The SCI mice treated with PBS or AP-EXO exhibited few or no axons at the lesion core (Fig. 4h and i, Supplementary Fig. 3c). Interestingly, axon dieback of CST fibers above the injury site, typically seen in SCI mice, was significantly reduced after AP-EXO or AP-EXO$_{R\&L\&S}$ treatment (Supplementary Fig. 3c). We also analyzed axonal regeneration across the injured region. In contrast to the naïve SCI mice and AP-EXO treated SCI mice, robust axonal regrowth was facilitated in AP-EXO$_{R\&L\&S}$-treated mice. This regrowth passed through the proximal astrocyte border, lesion core, and distal astrocyte border and penetrated to approximately 1500 μm beyond the lesion core (Fig. 4h and i). We examined transverse sections to visualize sprouted BDA positive fibers below the lesion, AP-EXO$_{R\&L\&S}$-treated mice revealed approximately 15% spared tract tracer-labeled neurons compared with sham group (Fig. 4j and k), and BDA-positive neurons colocalized with the presynaptic marker Syn1 and were in apposition with the postsynaptic marker postsynaptic density protein 95 (PSD95) (Fig. 4l). Additionally, AP-EXO$_{R\&L\&S}$ also promoted vesicular glutamic acid decarboxylase 67 (GAD67)-and vesicular glutamate transporter 1 (vGlut1)-positive boutons (putative inhibitory and excitatory synapses) apposing to ChAT below the injury site, as shown by multifluorescent orthogonal three-dimensional (3D) confocal images (Fig. 4m–n). While in PBS- or AP-EXO-treated mice, no BDA positive neurons or their contact to Syn1 or PSD95 were detected (Supplementary Fig. 3d). Similarly, neither the contact between ChAT and GAD67 nor vGlut1-positive boutons and BDA positive fibers were detectable. Taken together, these results indicated a reorganization of the spinal circuit and synaptic plasticity between CST motor-neurons and inhibitory or excitatory neurons, especially vGlut1, which have previously been associated with improvements in functional recovery [28,29].

Moreover, motor function recovery in AP-EXO$_{R\&L\&S}$-injected SCI contusion mice was evidenced by BMS scores and gait analysis. Firstly, to determine the best ratio of peptides to AP-EXO in SCI treatment, we generated the incubation mixture of AP-EXO and peptides to a mass ratio of 1:1 and 1:3 to form the AP-EXO$_{RVG\ (1:1)}$, AP-EXO$_{RVG\ (1:3)}$, AP-EXO$_{ILP\ (1:1)}$, AP-EXO$_{ILP\ (1:3)}$, AP-EXO$_{ISP\ (1:1)}$ and AP-EXO$_{ISP\ (1:3)}$ and injected into contused SCI mice. Hindlimb movement was measured in all independent experimental groups using open-field locomotion tests and the BMS scores [30–32] over the postinjury period, the BMS score dropped down to 0 in all animals at day 1 after injury (Fig. 5a, Supplementary Figs. 4a and 4c, e-g). Conversely, the animals in the PBS- or AP-EXO- treated control group developed only slight ankle movements such as spasms and resulting in an average final score of less than 2 (Fig. 5a, Supplementary Figs. 4a and 4c, 4e-g). Further functional evaluation revealed that significant recovery of locomotion began in the 1st week after AP-EXO$_{R\&L\&S}$ treatment (Fig. 5a, Supplementary Fig. 4c, 4e-g) and reached a BMS score up to ~4 in the 6th week (Fig. 5b). Functional recovery was shown as the restoring plantar stepping with full hindlimb weight support, followed by lift-off, forward limb advancement, and the reestablishment of weight support at initial contact in most of the animals (Fig. 5a and b). Fifty percent of AP-EXO$_{R\&L\&S}$ -treated animals achieved BMS score of ~4 and ≥ 40% reached a BMS score of ~3 (Fig. 5c). AP-EXO or single peptide modified AP-EXO (AP-EXO$_{RVG\ (1:1)}$, AP-EXO$_{RVG\ (1:3)}$, AP-EXO$_{ILP\ (1:1)}$, AP-EXO$_{ILP\ (1:3)}$, AP-EXO$_{ISP\ (1:1)}$ and AP-EXO$_{ISP\ (1:3)}$) slightly enhanced locomotor movement, with an average BMS score of ~2 (Supplementary Figs. 4c–d), and 3-folds mass of peptides linked to AP-EXO showed the equivalent motor function enhancement to that of equal mass ratio of peptides to AP-EXO (Supplementary Figs. 4a–b). Moreover, we used a footprint analysis system to assess and quantify detailed locomotion at the end timepoint. Mice were evaluated on a Catwalk XT system and gait recordings were made while the mice passed through the illuminated ceiling. In mice treated with AP-EXO$_{R\&L\&S}$, coordination movement of forelimbs and hindlimbs was observed (Fig. 5d, Supplementary Video 1-4), unfortunately, all SCI mice failed to show any hind paw placement. Interestingly, swing duration of both the forelimb and the hindlimb were decreased after spinal cord contusion but increased in 6 weeks after AP-EXO$_{R\&L\&S}$ implantation, especially for the hindlimb. Consequently, the hindlimb swing duration and base of support significantly increased following treatment (Fig. 5e and f). Stride length decreased significantly in the forelimb following a contusion injury and recovered after treatment to an extent of over 1.5 times compared with the SCI controls (Fig. 5g). Additionally, AP-EXO$_{R\&L\&S}$ treatment significantly enhanced multiple parameters of functional restoration, such as the stand time

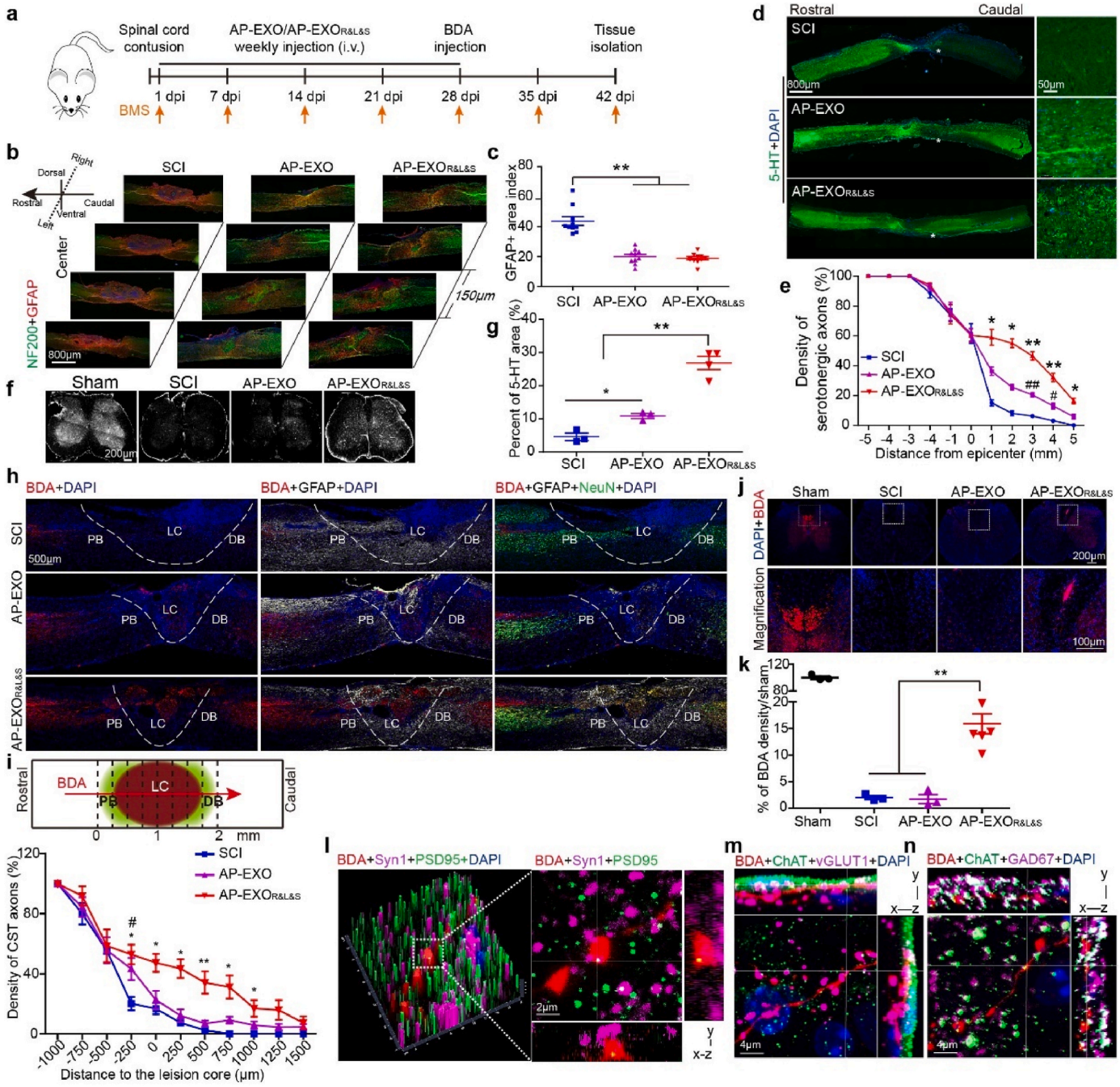

(caption on next page)

Fig. 4. AP-EXO$_{R\&L\&S}$ enables axon regeneration after spinal cord contusion in SCI mice. Adult mice were subjected to spinal cord contusion and received intravenous injections of AP-EXO or AP-EXO$_{R\&L\&S}$ beginning at day 1 after contusion at a dose of 1 mg/kg/week for 5 weeks. Four weeks after injury, BDA was intra-cortically injected to trace CST axons and tissues were harvested 2 weeks post BDA injection. **(a)** Timeline of the dose regimen for AP-EXO and AP-EXO$_{R\&L\&S}$ in treating spinal cord contused mice. **(b)** Immunostaining of NF200-positive neuro-filaments and GFAP-positive astrocytes in serial sagittal sections of the injured area. Scale bar: 800 μm. **(c)** Quantification of the GFAP-positive area in the injured center (SCI: n = 10, AP-EXO: n = 10, AP-EXO$_{R\&L\&S}$: n = 10, $^{**}p < 0.001$, One way ANOVA post Student-Newman-Keuls test). **(d–e)** Regenerating serotonergic axons in sagittal spinal cord sections after AP-EXO$_{R\&L\&S}$ treatment. **d**, representative images of regenerating serotonergic axons beyond the lesion site (asterisk). Scale bar: 800 μm, inset: 50 μm. **e**, quantification of regenerating serotonergic axons at indicated distance beyond the lesion (SCI: n = 7, AP-EXO: n = 7, AP-EXO$_{R\&L\&S}$: n = 7. $^{*}p < 0.05$, $\#p < 0.05$, one-way ANOVA on ranks post Tukey Test, $^{**}p < 0.001$, $\#\#p < 0.001$, one-way ANOVA post Student-Newman-Keuls test, * denominated as comparison between the SCI group and the AP-EXO$_{R\&L\&S}$ group, # denominated as comparison between the SCI group and AP-EXO group). **(f–g)** Projection of 5-HT-positive serotonergic axons of injured mice after AP-EXO$_{R\&L\&S}$ treatment at the L1 level. **f**, representative images of projected serotonergic axons. Scale bar: 200 μm. **g**, percent area coverage of 5-HT to total L1 transection (SCI: n = 3, AP-EXO: n = 3, AP-EXO$_{R\&L\&S}$: n = 4. $^{*}p < 0.05$, $^{**}p < 0.001$, one-way ANOVA post Student-Newman-Keuls test). **(h)** Sagittal spinal cord sections of the three treated groups showing BDA-labeled CST axons on composite tiled scans. Sections were also stained for cell nuclei (DAPI, left), astrocytes (GFAP, middle) and mature neurons (NeuN, right). Dot line demarcates astrocyte proximal (PB) and distal (DB) borders around the lesion core (LC). Scale bar: 500 μm. **(i)** Top, schematic of the lesion site and vertical lines used to count the density of axons crossing over each location indicated. Bottom, axon density of CST fibers. (SCI: n = 6, AP-EXO: n = 6, AP-EXO$_{R\&L\&S}$: n = 6. $^{*}p < 0.05$, $\#p < 0.05$, $^{**}p < 0.001$, −250 μm, 0 μm, 500 μm, one-way ANOVA post Student-Newman-Keuls test. 250 μm, 750 μm, 1000 μm, one-way ANOVA on ranks post Tukey test, * denominated as comparison between the SCI group and the AP-EXO$_{R\&L\&S}$ group, # denominated as comparison between the SCI group and the AP-EXO group). **(j–k)** Transverse spinal cord sections of projected BDA-labeled CST axons below the injury level after treatment. **j**, representative images of BDA-labeled CST axons below the injury site. Scale bar: 200 μm, inset: 100 μm. **k**, the comparison of BDA-positive CST axons below the injury site across 3 groups (sham: n = 3, SCI: n = 3, AP-EXO: n = 3, AP-EXO$_{R\&L\&S}$: n = 6. $^{**}p < 0.001$, one-way ANOVA post Student-Newman-Keuls test). **(l)** BDA-labeled terminals (red) beyond the lesion overlapped with the presynaptic (purple) and postsynaptic (green) markers synaptophysin (Syn1) and postsynaptic density protein 95 (PSD95), respectively. Scale bar: 2 μm. **(m–n)** BDA-labeled terminals (red) juxtaposed with ChAT-positive motor neurons (green) and vGLUT1-positive boutons (purple) or GAD67-positive boutons (purple) below the injury. Scale bar: 4 μm. vGLUT1, vesicular glutamate transporters. GAD67, glutamic acid decarboxylase 67.

(increased by 30-fold), maximum contact area (increased by 25-fold), and average swing speed (increased by 15-fold) of the hind paws touch the glass plate compared with SCI controls (Fig. 5h–j). Finally, we used motor-evoked potential (MEP) to evaluate neurological recovery and found that the peak-to-peak amplitude was increased in the AP-EXO$_{R\&L\&S}$ group compared with the control group (Fig. 5k). Thus, these results illustrated that AP-EXO$_{R\&L\&S}$ dramatically rescued locomotor function loss caused by spinal cord contusion. To clarify whether AP-EXO$_{R\&L\&S}$ could promote the functional blood vessels formation, we detected the existence of the CD31 positive cells in the injured center. The AP-EXO$_{R\&L\&S}$-treatment led to a significant increase of CD31 positive blood vessels than other groups. And the AP-EXO alone led to a very modest but significant blood vessel formation compared with that observed in PBS-treated SCI group (Supplementary Fig. 3e). Moreover, we also detected the inflammation status by quantitative analysis of CD68 positive macrophage after AP-EXO$_{R\&L\&S}$ treatment. The results showed that compared with the PBS-treated SCI group, CD68 positive macrophage was significantly decreased in both AP-EXO- and AP-EXO$_{R\&L\&S}$-treatment group (Supplementary Fig. 3f). Collectively, these data indicated that AP-EXO$_{R\&L\&S}$- treatment could promote vascular formation and alleviate inflammation after SCI.

2.4. AP-EXO$_{R\&L\&S}$ promotes robust axon regeneration in crushed SCI mice

We next tested whether our findings in contused SCI could be reproduced in spinal cord crush injuries, in which the lesion core pathophysiology has been proposed to be more suitable for neural regeneration. As expected, AP-EXO$_{R\&L\&S}$ significantly improved the BMS score of the crushed SCI mice to ~4 at the end of treatment (Fig. 6a–c) and enabled the robust regeneration of CST axons, with the longest axons across ≥3 mm (Fig. 6d–f). This effect was significantly compromised in AP-EXO-treated mice. Consistent with the findings shown in Fig. 4l–n, BDA-labeled terminals were overlapped with Syn1 and PSD95, and contacted ChAT-positive motor neurons and vGlut-1 or GAD67-boutons in the transverse section below the injured site in AP-EXO$_{R\&L\&S}$-treated mice, which reorganized the spinal circuit and synaptic plasticity (Fig. 6g–i).

2.5. Application and toxicity evaluation of bioactive peptide-loaded human plasma exosomes in nude mice with SCI

To probe more broadly the application of peptide-loaded exosomes, especially in the clinic, we isolated exosomes from human plasma (HP-EXO), and incubated them with RVG-CP05, ILP-CP05 and ISP-CP05. As demonstrated above, ≥75% of HP-EXO (Supplementary Fig. 5a) were loaded with the three peptides without altering the morphology or size of the HP-EXO (Supplementary Figs. 5b–c). The loaded HP-EXO (HP-EXO$_{R\&L\&S}$) was intravenously injected into nude mice with a dose regimen and treatment cycle similar to those in the above-mentioned research protocols. As expected, mice treated with HP-EXO$_{R\&L\&S}$ showed a higher BMS score after the first administration and the score enhanced gradually during the experiments (Fig. 7a). Likewise, locomotor and coordination function were quantified using parameters such as base of support for fore-and hind-limbs, stride length for forelimbs, the stand time and the maximum contact area for hindlimbs, all parameters were significantly elevated in HP-EXO$_{R\&L\&S}$-treated nude mice (Fig. 7b–f), indicating that HP-EXO$_{R\&L\&S}$ elicited functional rescue in nude mice with spinal cord contusion. Next, we detected the toxicity of HP-EXO$_{R\&L\&S}$ using markers of liver function such as alkaline phosphatase (ALP), alanine aminotransferase (ALT) and aspartate aminotransferase (AST) as well as markers of kidney function such as blood urea nitrogen (BUN), creatinine (CREA) and uric acid (UA). Neither liver function markers nor kidney function markers elevated after HP-EXO or HP-EXO$_{R\&L\&S}$ treatment (Fig. 7g and h). In addition, no morphological abnormality was found in kidney, liver, lung and spleen (Fig. 7i), indicating that HP-EXO$_{R\&L\&S}$ did not induce any liver, kidney, lung or spleen toxicity. To exclude the possibility that the inflammation response induced by loaded HP-EXO, CD3-positive T cells and CD68-positive macrophage were detected, the results displayed both of them didn't change after HP-EXO or HP-EXO$_{R\&L\&S}$ treatment (Fig. 7j). These data strengthen the conclusion that HP-EXO$_{R\&L\&S}$ elicits functional recovery following SCI without triggering any detectable toxicity and inflammation response.

3. Discussion

Recent years have witnessed the advent of promising strategies that combat the devastating effects of SCI. However, these treatment schemes produce limited non-functional recovery and make secondary injury to spinal cord in animal models that could hamper their implementation into the clinic. In this study, we developed an AP-EXO-based biological scaffold by anchoring neuron-targeting and growth-facilitating peptides, which greatly improved the targeting specificity and therapeutic efficacy of bioactive peptides. This scaffold possessed three major advantages against SCI including non-secondary injury to

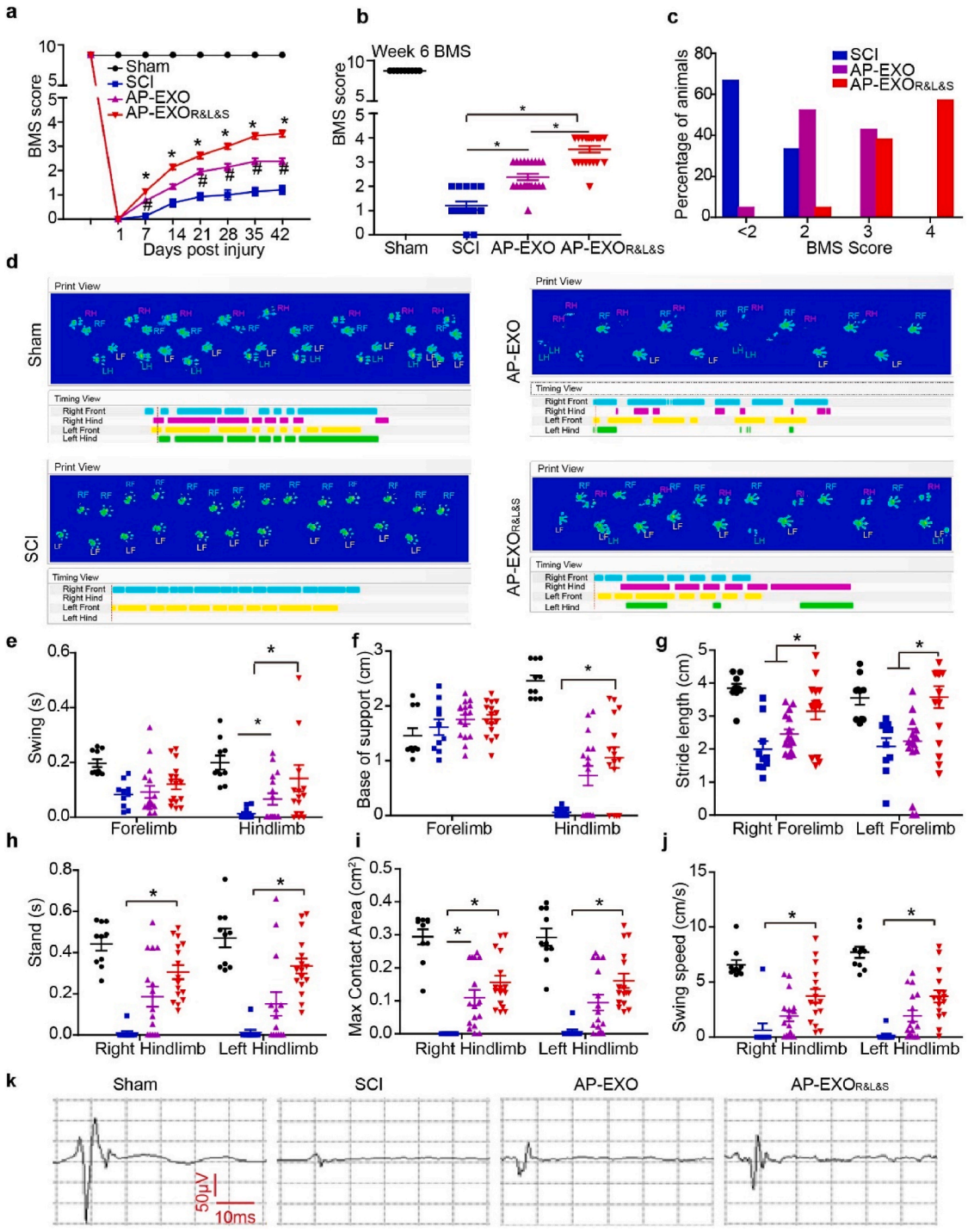

Fig. 5. Functional recovery after AP-EXO$_{R\&L\&S}$ treatment in contused SCI mice. Adult mice were subjected to spinal cord contusion and received intravenous injections of AP-EXO or AP-EXO$_{R\&L\&S}$ beginning at day 1 after contusion at a dose of 1 mg/kg/week for 5 weeks. The BMS scores of mice were then determined weekly for 6 weeks. Four weeks after injury, BDA was intra-cortically injected to trace CST axons. One day before tissue extraction, gait analysis of the mice was performed. **(a–c)** BMS scores of spinal-cord-contused animals treated with AP-EXO or AP-EXO$_{R\&L\&S}$ (sham: n = 9, SCI: n = 15, AP-EXO: n = 21, AP-EXO$_{R\&L\&S}$: n = 21, sham group designated as the mice received laminectomy without contusion injury, SCI group designated as mice injected with PBS, AP-EXO group designated as mice injected with autologous mouse exosomes, and AP-EXO$_{R\&L\&S}$ group indicated the mice injected with peptide-painted exosomes). **a**, BMS score assessment over time (*$p < 0.05$, #$p < 0.05$, one-way ANOVA on ranks post Dunn's Method, * designated as comparison between the SCI group and the AP-EXO$_{R\&L\&S}$ group, # designated as comparison between the SCI group and the AP-EXO group). **b**, BMS score at week 6 after spinal cord contusion (*$p < 0.05$, one-way ANOVA on ranks post Dunn's Method). **c**, percentage of animals at successive score segments after treatment. **(d–j)** Catwalk gait analysis to determine the locomotor recovery after AP-EXO or AP-EXO$_{R\&L\&S}$ treatment (sham: n = 10, SCI: n = 10, AP-EXO: n = 16, AP-EXO$_{R\&L\&S}$: n = 16). **d**, representative images of footprints after AP-EXO$_{R\&L\&S}$ treatment. **e**, swing duration for fore-and hind-limb after AP-EXO or AP-EXO$_{R\&L\&S}$ treatment (*$p < 0.05$, one-way ANOVA on ranks post Dunn's Method). **f**, base of support for fore-and hind-limbs (*$p < 0.05$, one-way ANOVA on ranks post Dunn's Method). **g**, stride length of the left and right forelimb (*$p < 0.05$, one-way ANOVA post Student-Newman-Keuls test). **h**, stand time of left and right hind-limbs (*$p < 0.05$, one-way ANOVA on ranks post Dunn's Method). **i**, maximum contact areas of left and right hind-limb (*$p < 0.05$, one-way ANOVA on ranks post Dunn's Method). **j**, average swing speed of the left and right hind-limbs (*$p < 0.05$, one-way ANOVA on ranks post Dunn's Method). **(k)** Examples of motor-evoked potential (MEP) recordings from mice at week 6 post-surgery.

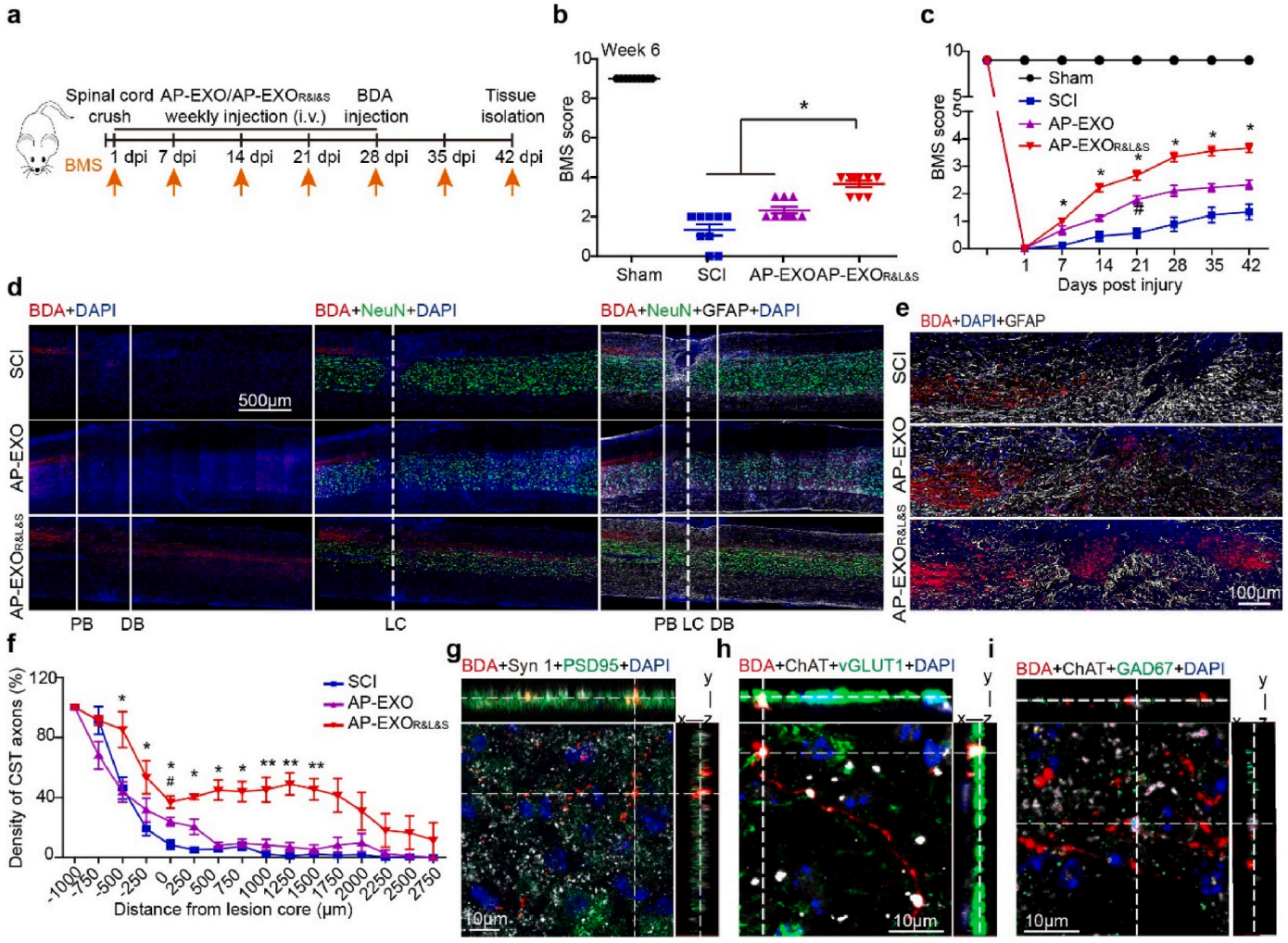

Fig. 6. Functional assays of AP-EXO$_{R\&L\&S}$ in the spinal cord crush model. Adult mice were subjected to spinal cord crush and received intravenous injections of AP-EXO or AP-EXO$_{R\&L\&S}$ beginning at day 1 after contusion at the dose of 1 mg/kg/week for 5 weeks. The BMS scores of the mice were then determined weekly for 6 weeks. Four weeks after injury, BDA was intra-cortically injected to trace CST axons **(a)** Schematic timeline of the dose regimen for the study of AP-EXO and AP-EXO$_{R\&L\&S}$ in spinal cord crush mice. i. v. Is short for intravenous injection. **(b–c)** BMS score assessment of spinal cord crush mice treated with AP-EXO or AP-EXO$_{R\&L\&S}$. **b**, BMS scores at the end of the treatment. **c**, BMS scores in consecutive week. (SCI: n = 9, AP-EXO: n = 9, AP-EXO$_{R\&L\&S}$: n = 9. $*p < 0.05$, $\#p < 0.05$, One way ANOVA on ranks post Turkey test). **(d)** Sagittal spinal cord sections of the three treated groups showing BDA-labeled CST axons on composite tiled scans. Sections were also stained for cell nuclei (DAPI, left), mature neurons (NeuN, middle) and astrocytes (GFAP, right). Solid lines demarcate astrocyte proximal (PB) and distal (DB) borders around the lesion core (LC). Scale bar: 500 μm. **(e)** Representative magnified images showing BDA-labeled CST regrowth across the proximal borders, sections were stained for astrocytes. Scale bar: 100 μm. **(f)** Axon density of CST fibers across the proximal and distal border. (SCI: n = 5, AP-EXO: n = 5, AP-EXO$_{R\&L\&S}$: n = 5. $*p < 0.05$, $\#p < 0.05$, $**p < 0.001$, −500 μm, −250 μm, 0 μm, 750 μm, 1000 μm, 1250 μm, 1500 μm, one-way ANOVA post Student-Newman-Keuls test. 250 μm, 500 μm, one-way ANOVA on ranks post Tukey test. *dominated as comparison between the SCI group and the AP-EXO$_{R\&L\&S}$ group, # denominated as comparison between the SCI group and the AP-EXO group). **(g)** BDA-labeled terminals (red) beyond the lesion overlapped with the presynaptic (white) and post-synaptic (green) markers synaptophysin (Syn1) and postsynaptic density protein 95 (PSD95), respectively. Scale bar: 10 μm. **(h–i)** BDA-labeled terminals (red) juxtaposed with ChAT-positive motor neurons (white) and vGLUT1-positive boutons (green) or GAD67-positive boutons (green) below the injury. Scale bar: 10 μm.

spinal cord, non-immunogenicity and greater therapeutic benefits, which elicited the robust axon regeneration and newly intraspinal circuits formation below the lesion level. In order to validate the effects and safety of exosomes from the plasma of healthy donors (HP-EXO) as peptides delivery vehicle, further research was carried out to generate the HP-EXO based therapeutic scaffold, HP-EXO$_{R\&L\&S}$ appeared the same effect as AP-EXO$_{R\&L\&S}$ in SCI model of nude mice without elicit adverse effect. These findings not only provide a novel noninvasive strategy for SCI treatment but also demonstrate the role of AP-EXO-based scaffold in promoting axon regeneration.

Our previous study has demonstrated that exosomes from various sources could be loaded by functional cargos via CP05 [20], and as delivery vehicles, blood exosomes are potential source of safe and sufficient exosomes, as they integrate various membrane proteins including CD63 but without any cancer-stimulating activities [33,34]. Whereas one of challenges to propel the clinical translation is the origin of exosomes [35]. Autologous plasm derived exosome is readily available and also avoid immunological reactions associated with foreign exosomes. Besides, exosomes of autologous origin have come into existence due to their strength of safety and efficiency in mice model [36] and clinical trials [37]. Meanwhile, studies have demonstrated exosomes derived from blood were generated higher yields and of preferable size than exosomes from cell lines, which may facilitate their intracellular delivery [38]. As a result, we used autologous exosomes from plasma as delivery vehicle in this study, these AP-EXO was *in vivo* loaded with neuron-targeting (RVG) and axon growth-facilitating peptides (ILP and ISP), and finally they were reinfused and absorbed into the target sites of injury without inducing the immunogenicity upon treatment. Although

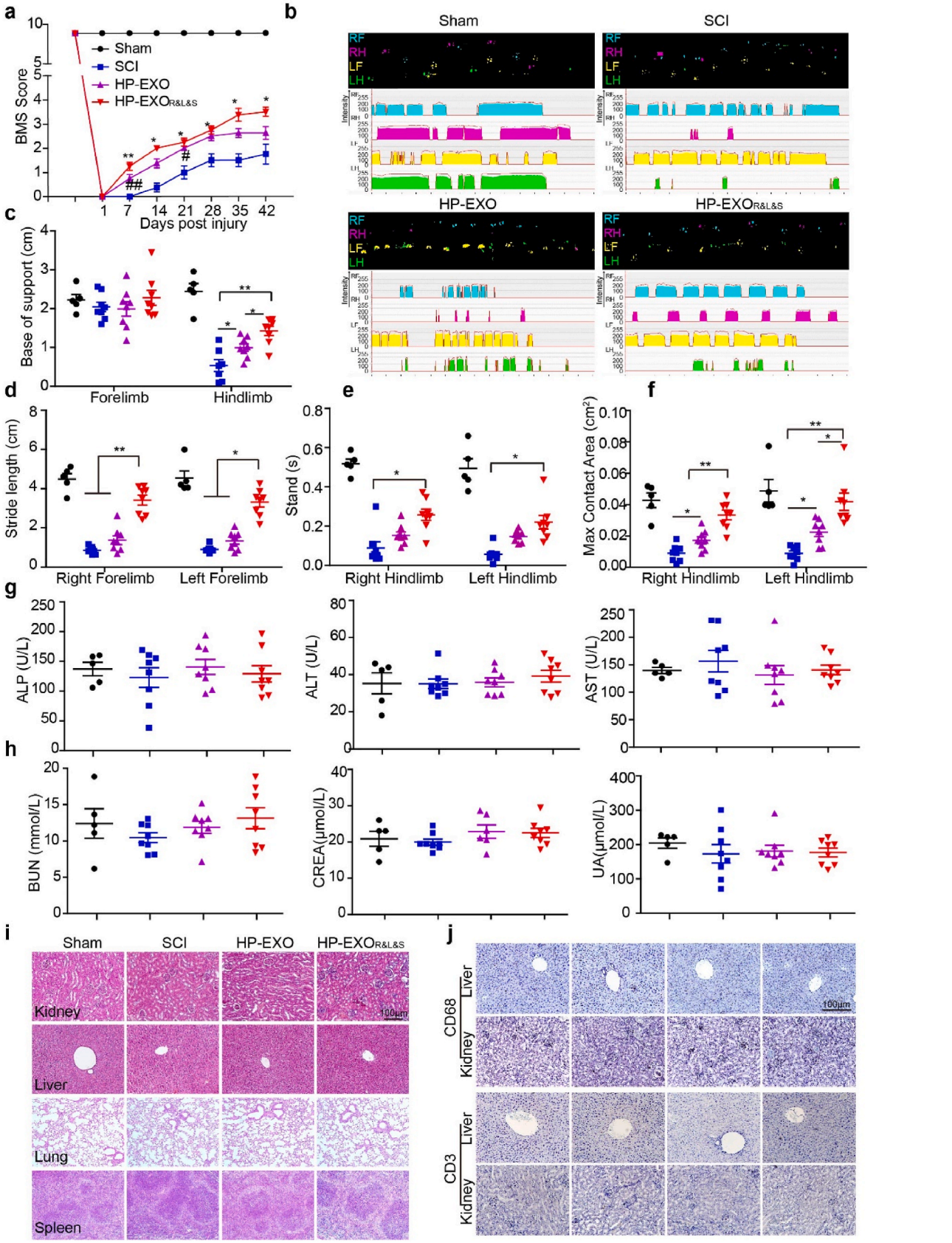

(caption on next page)

Fig. 7. Systemic evaluation of HP- $EXO_{R\&L\&S}$ in nude mice with spinal cord contusion. Nude mice were subjected to spinal cord contusion and then intravenously injected with HP-EXO or HP-$EXO_{R\&L\&S}$ at a dose of 1 mg/kg/week for 5 weeks starting at day 1 after contusion. BMS scores were assessed over time. Gait analysis was conducted 1 day before tissue collection. (a, c-h, sham: n = 5, SCI: n = 8, HP-EXO: n = 8, HP-$EXO_{R\&L\&S}$: n = 8). **(a)** BMS scores of contused nude mice treated by HP-EXO or HP-$EXO_{R\&L\&S}$ (*$p < 0.05$, #$p < 0.05$, one-way ANOVA on ranks post Tukey Test, **$p < 0.001$, ##$p < 0.001$, one-way ANOVA post Student-Newman-Keuls test, *dominated as comparison between the SCI group and the HP-$EXO_{R\&L\&S}$ group, # denominated as comparison between the SCI group and the HP-EXO group). **(b–f)** Gait analysis of mice treated with HP-EXO or HP-$EXO_{R\&L\&S}$. **b**, representative footprint images of contused mice treated with PBS, HP-EXO or HP-$EXO_{R\&L\&S}$. **c**, base of support for forelimbs and hindlimbs after treatment (*$p < 0.05$, **$p < 0.001$, one-way ANOVA post Student-Newman-Keuls test). **d**, stride length of the left and right forelimbs (**$p < 0.001$, one-way ANOVA post Student-Newman-Keuls test, *$p < 0.05$, one-way ANOVA on ranks post Dunn's Method). **e**, stand time of left and right hindlimb (*$p < 0.05$, one-way ANOVA on ranks post Dunn's Method). **f**, max contact area of left and right hindlimb (*$p < 0.05$, **$p < 0.001$, one-way ANOVA post Student-Newman-Keuls test). **(g)** measurement of plasma ALP, ALT and AST enzymes in sham controls, PBS treated SCI controls, and SCI mice treated with HP-EXO or HP-$EXO_{R\&L\&S}$. **(h)** measurement of plasma BUN, CREA or UA in sham controls, PBS treated SCI controls, and SCI mice treated with HP-EXO or HP-$EXO_{R\&L\&S}$. **(i)** hematoxylin and eosin (H&E) staining of kidney, liver, lung and spleen tissue sections from sham controls, PBS treated SCI controls, and SCI mice treated with HP-EXO or HP-$EXO_{R\&L\&S}$. Scale bar:100 μm. **(j)** Immunohistochemistry for CD3-positive T lymphocytes and CD68-positive macrophages in the kidney and liver from sham controls, PBS treated SCI controls, and SCI mice treated with HP-EXO or HP-$EXO_{R\&L\&S}$. Scale bar: 100 μm.

it is hard to speculate which kind of individual peptide in the AP-$EXO_{R\&L\&S}$ mixture are mainly involved in the therapeutic outcomes and contributed predominantly to the neural regeneration and functional recovery. Our forthcoming study will be focusing on the underlying molecular mechanisms of neural regeneration and functional recovery in details and understand the role of individual peptides on the therapeutic outcome against SCI. The results we showed in this study suggested that RVG, ILP and ISP combined together to repair the SCI damage where three of them coordinate and compensate each other to maximize their effects. For example, RVG could directly enhance AP-EXO homing into neurons of spinal cord via binding to p75NTR, this interaction is even faster and more efficient than the binding of nerve growth factors (NGF), an endogenous p75NTR ligand to p75NTR [23]. Interestingly, binding of RVG to p75NTR may activate the retrograde transport machinery and facilitate neurotrophic factors retrograde delivered into the brain and spinal cord [39], thus enhance neuronal survival and regeneration. Furthermore, our previous studies showed that the existence of peptide in the circulation is prolonged to 6 h when loaded onto exosomes [20,40], and in this study, we have detected a prolonged localization of AP-$EXO_{R\&L\&S}$ in the injured spinal cord. We assumed that tethered peptides of ILP and ISP to AP-EXO enabled their spinal cord localization, serum stability and inhibitory efficacy to CSPGs or PTPσ. Notably, in the bioactive scaffold of AP-$EXO_{R\&L\&S}$ we generated, the peptides ILP and ISP also served as targeting moieties due to binding to LAR and PTPσ expressed on the surface of neurons. Therefore, in our research, ILP and ISP possess dual roles in both homing ability and growth-facilitating potency. Interestingly, we noticed that both LAR and PTPσ, to which ILP and ISP bind, were expressed on both serotonergic neural fibers and CST fibers, consequently, robust axon regrowth of both 5-HT-positive and BDA-labeled fibers were detectable across the lesion site. Additionally, recent studies reported that ISP enhanced remyelination and recovery in an experimental autoimmune encephalitis mouse model [24], further providing vital clues in the extended beneficial effect of this AP-$EXO_{R\&L\&S}$. Another significant advantage of AP-EXO-based scaffolds compared with other exosomes from autologous cells such as neural stem cell is it is easy to acquire, thus facilitates the translational and clinical application. Taken together, the use of autogenously derived exosomes provides vital clues in personalized treatment scheme [36,41] for SCI recovery.

As is known, the development of therapeutics for SCI is complicated because of limited axon growth ability and penetration of BSCB, which prevents certain drugs and large molecule entering the spinal cord. As a novel tool, exosome has been reported in treating neurological condition [42] and surface modification with RVG could increase exosomes uptake by two-fold in brain [43,44]. In our study, we found that the majority of AP-EXO localized in the liver and few accumulated in the injured spinal cord after intravenous injection. Therefore, we have boosted the targeting ability of AP-EXO after loading RVG peptide to increase their therapeutic effects in SCI. As expected, we noticed that RVG facilitated AP-EXO home to the spinal cord tissue either in wild type mice or contused SCI mice. Surprisingly, we observed that abundance of RVG modified AP-EXO was aggregated in the SCI injury center other than the normal tissue of non-injured region. It is possible that the BSCB was transiently compromised after injury [45] due to the immediate, non-specific vascular changes and make it easier to cross the BSCB. Interestingly, in this study, we observed the reduction of injured area and increased functional recovery in AP-EXO-treated SCI mice, with the equivalent functional recovery levels of NSC-EXO at the same dosage (data were not shown). Considering that both AP-EXO and NSC-EXO share a large number of common therapeutic molecules such as neural cell adhesion molecule 1 (NCAM) and 14-3-3 [25] family proteins involved in endocytosis, cell growth, axon guidance and synapse formation (data were not shown), we speculate that similar to the underlying mechanism of exosomes derived from other origins in treating cardiovascular disease [46], it is likely that AP-EXO modulates the microenvironment of the injury site to alleviate the injury degree. And our forthcoming studies will focus on exploring the underlying mechanisms of AP-EXO, especially in modulating the liver-spinal cord axis in alleviating the extrinsic inhibitory barrier in the injured area and promoting functional recovery in SCI mice. Despite the AP-EXO has shown therapeutic promise in SCI mice, recovery remains incomplete as BMS score of the AP-EXO-treated mice reached to ~2, indicating that functional recovery after SCI possibly induce the neuron-intrinsic growth capacity apart from removal of the extrinsic inhibition barrier. Thus, it is becoming apparent that combination of various functional cargos will be required. Moreover, AP-$EXO_{R\&L\&S}$ could be delivered through tail vein, thus, this treatment paradigm does not involve the invasion of the spinal cord and thereby avoids complications associated with injury secondary to local transplantation. As a proof of validation, we isolated exosomes from healthy human plasma and loaded with combinatory peptides have demonstrated functional rescue and reliable security *in vivo*, hence, it provides the premise and guarantee for the feasibility of future clinical translational research. Regarding the clinical implications of the delivery system demonstrated in our study, some important factors should be taken into consideration including exosome concentration, effective delivery targeting SCI lesion site with "escaping depletion" at destination and side effects to the central nervous system. According to previous clinical trials and our research data in this study, AP-$EXO_{R\&L\&S}$ was recommended administered at the dose of 1 mg/kg and intravenously injected into the SCI patients. Studies have reported that exosomes could be up-taken and delivered into receptor cells through membrane fusion, endocytosis or cell targeting patheways [47].

Our research in SCI mice showed that AP-$EXO_{R\&L\&S}$ could be targeted delivered into neurons and sustain for 7 days in the injured spinal cord, indicating the injection cycle of 1 week for AP-$EXO_{R\&L\&S}$ was optimal. Although we have verified the safety of liver, kidney, spleen and lung in nude mice, we need to further verify the safety and side effects especially in the central nervous system (CNS) in the follow up study, including whole-body tolerance and evaluation of CNS function and corresponding behavior to identify the potential side effects on brain after administration. Due to exosomes could be distributed in liver and lung after intravenous injection, more attention should be paid in

dispersing the AP-EXO$_{R\&L\&S}$ to ensure no aggregation was presented and avoid venous embolism.

Overall, taking advantages of autogenously derived exosomes and the targeting delivery system, we provide a novel and safe approach for improving motor function recovery after SCI. Our study highlights three unique advantages of the AP-EXO-based scaffold for SCI treatment: (i) the autologous derived exosomes are immune privileged with safety; (ii) compared with the *trans*-spinal cord delivery approach, this targeting delivery system avoid secondary injury to spinal cord; (iii) the AP-EXO-based scaffold exhibits high efficacy for treating SCI as the AP-EXO and peptides are coordinate and compensate each other. Mechanically, the AP-EXO provides stable platform for peptides, and complementarily, the peptides enhance the therapeutic potency. A limitation of this study is that although we have clearly demonstrated the efficacy and safety of AP- EXO$_{R\&L\&S}$ in contusion and crush SCI mice model, further studies in large animal models, such as canine, porcine or nonhuman primate models, are warranted. In summary, we developed a novel multi-peptides-modified autologous exosome preparation loaded with combinatory bioactive peptides directly targeting to spinal cord injury sites that potentiated robust axon growth and SCI repair and thus provides new insights into targeted and noninvasive SCI treatment strategies. The finding in this study will be helpful to expand the application of combinatory peptides and human plasma derived autologous exosomes in promoting regeneration and recovery upon SCI treatment.

4. Materials and methods

4.1. Isolation and culture of cortical primary neurons

Primary neurons were harvested from brain cortex of embryos of C57BL/6 mice (purchased from Vital River Laboratory Animal Technology Co., Ltd.) with gestational day 16 as previously described [48,49]. Pregnant mice were sacrificed humanely and sterilized with 70% pre-cool ethanol, all the animal experiments were approved by the Ethics Committee of Shandong University (Jinan, Shandong, China; ECSBMSSDU2021-2-014). Cortical parts of the brain were dissected under the stereomicroscope (Chongqing Optec Instrument Co., Ltd., Chongqing, China) and cut into the approximately 1 mm^3 of pieces. Tissues were then dissociated with 0.2% (w/v) papain (LS003119; Worthington Biochem, Lakewood, NJ, USA) and 0.004% (w/v) DNase solution at 37 °C for 30 min. During digestion, the tissue was gently pipetted 8–10 times every 10 min. After digestive enzyme totally inactivated, the tissue was centrifuged at 200×*g* for 5 min and then all suspended were carefully aspirated and filtered through a 70 μm cell strainer (BD Biosciences) to filter cell lumps. The cells were resuspended in medium (Dulbecco's modified Eagle's medium, Invitrogen; 10% Fetal Bovine Plasma; 1% penicillin-streptomycin). Following counted, the cells were seeded into suitable wells precoated with poly-D-lysine (P4707; Sigma-Aldrich, St. Louis, MO, USA). After 4 h, half of the medium was replaced with neuronal medium (Neurobasal; 2% B27 supplement, Invitrogen; 1 mM l-glutamine, Invitrogen; 1% penicillin and streptomycin, Invitrogen). Subsequently, half of the neuronal medium was replaced every 3 days until needed for advanced experiments.

4.2. Exosome extraction and identification

(1) Exosome isolation

Exosomes were isolated using the sequentially centrifugal methods, briefly, cell culture medium from neural stem cells was sequentially centrifuged at 1000×*g* for 10 min, followed by 10000×*g* for 30min. The supernatant was collected and filtered with a 0.22 μm filter (Millex, Germany), followed by ultracentrifugation at 100,000×*g* for 70 min to pellet exosomes. Exosome pellets were washed in a large volume of PBS and recovered by centrifugation at 100,000×*g* for 70 min. The total protein concentration of exosomes was quantified by the BCA assay (Thermo, US). For plasma exosomes isolation, autologous mouse plasma was collected from medical canthal venous plexus of healthy mice before spinal cord injury models were established, and human plasma was obtained from healthy volunteers (all the human experiments were approved by the Ethics Committee of Tianjin Medical University General Hospital, Tianjin, China; IRB2020-YX-011-01), plasma was centrifuged at 3000×*g*, 6000×*g* and 10000×*g* twice for 30 min each time to remove the cell debris. The supernatant was diluted 10 times with 1 × PBS and transferred into a fresh tube, filtered with a 0.22 μm filter, the supernatant was subjected to the ultra-speed centrifuge (Beckman Optima L-100 XP, Beckman Coulter) and pelleted by ultracentrifugation at 100,000×*g* for 70 min, then exosome pellet was washed with a large volume of PBS and recovered by centrifugation at 100,000×*g* for 70 min.

(2) Characterization of exosomes

The size of exosomes was measured by Nano Particle Tracking and eta potential distribution analyzer (NS300, Malvern, UK). The morphology of exosomes was visualized with a high-resolution transmission electron microscope (Hitachi HT7700, Japan). The procedure for exosome preparation for transmission electron microscopy as the same as previously described [20,50]. Briefly, exosomes or exosomes linked with peptide pellet was fixed in 2% (w/v) paraformaldehyde, and deposited on formvar-carbon coated EM grids for 20 min in a dry environment. Excess solution was blotted off and the grids were washed by 100 μl PBS and the refixed with 50 μl drop of 1% glutaraldehyde for 5 min, the girds were then washed with distilled water for eight times (2 min for each time). Subsequently, the grids were transferred to a 50 μl drop of uranyl-oxalate solution (pH = 7) for 5 min and then to a 50 μl drop of methyl cellulose-UA for 10 min on ice. The excess solution was blotted off, and the sample was dried and observed under the electron microscope at 80 kV.

(3) Immunogold staining of His-CP05 binding with exosomes

Ten microgram autologous exosomes from plasma were incubated with 10 μg His-CP05 at 4 °C for 6 h, the non-specific and unbound peptides were washed with PBS for five times in a 2-ml ultracentrifuge tubes and filtrated with 100-Kd diafiltration tube (Millipore). Subsequently, His-CP05-exosomes complexes (AP-EXO$_{CP05\text{-}His}$) were resuspended in 20 μL PBS and mixed with an equal volume of 4% (w/v) paraformaldehyde. AP-EXO$_{CP05\text{-}His}$ were absorbed on electron-microscope grids and washed with PBS/50 mM glycine for four times, and the blocked with PBS/5% (w/v) BSA for 10 min at room temperature. Subsequently, the complexes were incubated with His primary antibody (1:200, Santa Cruze, sc-8036, diluted with 1% BSA) for 30 min, washed with washing buffer (PBS/0.1% BSA) for 6 times (3 min for each time), and labeled with protein A-gold conjugates (1:500, UMC Utrecht, UA-PAG10, The Netherlands) for 20 min. Then the complexes were stained with uranyl-oxalate solution (pH 7) and methyl cellulose-UA and observed under the electron microscope at 80 kV, as described above.

(4) Western blot of exosomes

Exosome pellets were lysed in lysis buffer (125 mM Tris-HCl, pH6.8, 10% sodium dodecyl sulfate (SDS), 2 M urea, 20% glycerol and 5% 2-mercaptoethanol) and subjected to 10% SDS-polyacrylamide gel electrophoresis. The protein was transferred to PVDF membranes and membranes were blocked with 5% skimmed milk and probed with different primary antibodies including Alix antibody (1:1000, Cell Signaling Technol., US), CD63 (1:200 Santa Cruze, US) and CD81 (1:200, Santa Cruze, US). bounded primary antibodies were detected by peroxidase-conjugated rabbit anti-mouse, goat-*anti*-rabbit, respectively. The bands were developed by ECL western blot analysis system (Millipore, Billerica, MA).

4.3. Peptide preparation

Naked peptides and fluorescence labeled peptides were synthesized commercially with a purity>95% by Chinapeptide Co. Ltd. Lyophilized peptides were dissolved in sterile water and stored at −80 °C until use. Peptide sequences are as follows:

RVG, YTIWMPENPRPGTPCDIFTNSRGKRASNG;

RVG-CP05: YTIWMPENPRPGTPCDIFTNSRGKRASNGGGGSCRHSQMTVTSRL;

ILP, NH2- DLADNIERLKANDGLKFSQEYESI;

ILP-CP05, NH2-DLADNIERLKANDGLKFSQEYESIGGGSCRHSQMTVTSRL;

ISP, NH2-DMAEHMERLKANDSLKLSQEYESI;

ISP-CP05, NH2- DMAEHMERLKANDSLKLSQEYESIGGGSCRHSQMTVTSRL.

4.4. Binding efficiency of exosomes to peptides

Binding affinity of peptides to exosomes were measured by flow cytometry as previously mentioned [20]. Briefly, FAM-labeled ILP-CP05 (10 μg), MCA-labeled ISP-CP05(10 μg) or Cy5.5-labeled RVG-CP05(10 μg) was incubated with exosomes (10 μg) derived from mouse or human plasma at 4 °C for 6 h individually or together and washed with PBS for five times in 2-ml ultracentrifuge tubes, followed by filtration with diafiltration tubes (Millipore) to remove unbound peptides as described above. The complexes were subjected to flow cytometry (BD LSRFortessa, US). To analyze triple-modification efficiency of peptides to exosomes, MCA-ISP-CP05 and Cy5.5- RVG-CP05 double positive exosomes were selected firstly, and FAM- ILP-CP05 positive exosomes were analyzed in the double-positive exosomes group.

To visualize multi-modification of exosomes, autologous exosomes from plasma (30 μg) labeled with DiR dye (Life Technologies) as per the manufacturer's instruction were preincubated with FAM-labeled ILP-CP05 (30 μg), rhodamine - labeled ISP-CP05 (30 μg), and Alexa Flour 405-labeled RVG-CP05 (30 μg) at 4 °C for 6 h, mixture of three peptides was used as control. Exosome-peptides complexes or peptides mixture were subjected to 100-Kd diafiltration tube (Millipore) and washed by PBS for five times to remove the unbound peptides. The samples were then resuspended with 50 μl PBS. Aldehyde sulfate beads (5 μl, Life Technologies) were added to the solution, mixture of the beads and exosomes was allowed to mix using a bench-top rotator for 15 min at room temperature. PBS (600 μl) was then added to the solution and mixing was continued overnight at 4 °C. Then 1 M glycine (400 μl) was added, and mixing was continued for 1 h at room temperature. The mixture was then spun down at 14,000 g at room temperature for 1 min, supernatant aspirated, and pellet resuspended in 200 μl PBS. Exosomes bounded to the beads were washed three times with PBS. Exosome-bounded beads were dropped onto the slides and under the scanning confocal laser microscopy (Zeiss 900, Germany).

4.5. Axonal guidance spot assays

CSPG gradients were prepared as described previously [22], briefly, circle microscope glass coverslips (15 mm, Fisher Scientific) coated with poly-L-lysine (Sigma-Aldrich, P6470) were spotted with 5 μl drop of different concentration of chicken CSPG (Millipore, CC117) with Texas Red in the center. Texas Red was used to visualize the interface. After the spots were allowed to dry, dissociated primary cortical neurons were seeded on the coverslips at a density of 8×10^4 cells for 2 days. For peptides and exosome-peptides complexes experiments, AP-EXO 10 μg alone or AP-EXO incubated with 10 μg RVG-CP05 ($AP\text{-}EXO_{RVG}$), ISP-CP05 ($AP\text{-}EXO_{ISP}$) or ILP-CP05 ($AP\text{-}EXO_{ILP}$) respectively or simultaneously, were added into the media after cell adhesion. Cells were fixed and stained with *anti*-βIII-tubulin antibody (1:1000, Abcam, ab41489), followed by the incubation with FITC-*anti*-chicken IgY antibody. Images were acquired on Olympus FV1000 inverted confocal microscope. Axonal outgrowth assays were performed as previously described, briefly, after the wells of 24-well plate were coated with the mixture of poly-L-lysine and chicken CSPG (2.5 μg/ml), dissociated primary cortical neurons were plated on the wells and incubated for 5 days at 37 °C. Neurons were stained with *anti*-βIII-tubulin primary antibody and the corresponding secondary antibody. Images were acquired using the Olympus inverted microscope and axonal length was measured using the ImageJ program.

4.6. Endocytosis of exosome into neurons

Co-culture of primary cerebral cortical astrocytes and neurons were performed as previously described [22]. Briefly, primary cultures of cerebral cortical astrocytes were prepared from newborn C57BL/6 mice, confluent cultures of astrocytes were cultured for 7 days and dissociated cerebral cortical neurons were plated on the monolayers for 48 h. Ten microgram Pkh26-labeled AP-EXO or $AP\text{-}EXO_{R\&L\&S}$ were added into the culture. Two-days after incubating, cells were fixed and stained with mouse *anti*-βIII-tubulin antibody (1:1000, Abcam, ab78078) and rabbit *anti*-ALDH1L1 (1:200, proteintech, 17390-1-AP) primary antibody and corresponding secondary antibody. Endocytosis of exosomes into astrocytes or neurons were detected using Olympus FV1000 inverted confocal microscope (Japan).

4.7. Mice spinal cord injury model

Female C57BL/6 and BALB/c nude mice (8–10 weeks old) were used for this study. The mice were purchased from Vital River Laboratory Animal Technology Co., Ltd. Animals were kept in an environment with a 12/12-h light-dark cycle with a temperature of 20–25 °C and humidity of 40%–60%. Mice were given food and water ad libitum. All experimental procedures involving animals were approved by the Ethics Committee of Shandong University (Jinan, Shandong, China; ECSBMSSDU2021-2-014). For surgical procedures of contusion model, mice were anesthetized with isoflurane (RWD, R510-22, Guangdong, China). The skin and fascia were cut longitudinally with T8 as the center, and then the muscles were gently dissected to expose the T7-T9 spinous processes. T8 laminectomy was performed, and the spinal cord was fully exposed. Spinous process fixators were used to fix the T7 and T9 spinous processes of mice. The NYU Impactor-III (WM Keck, USA) was then used to establish a moderate spinal cord contusion model (5 g × 12.5 mm). After confirming that the contusion was successful, the muscles, fascia, and skin were sutured. The bladder was manually emptied twice a day after SCI. Cefuroxime sodium (6 mg/ml, dissolved in saline; Hongtu, Nanjing, China) was administered by intramuscular injection to prevent urinary tract infection. The surgical of spinal cord crush injury was performed at T8 as previously described [51]. After the mice were anesthetized with isoflurane, the skin and fascia were cut longitudinally with T8 as the center, and then the muscles were gently dissected to expose the T7–T9 spinous processes. T8 laminectomy was performed, and the spinal cord was fully exposed. The spinal cord was then fully crushed for 2 s using forceps with the tip width of 0.1 mm. The tips were inserted into either side of the spinal cord and then crush dorsal aspect of spinal cord with a depth of 0.8 mm to ensure bilaterally sever the CST. The muscles, fascia, and skin were sutured.

4.8. Tissue distribution

To examine the biodistribution $AP\text{-}EXO_{R\&L\&S}$ in spinal cord injury mice model, DiR (Life Technologies) labeled AP-EXO was used. Briefly, DiR labeled AP-EXO (30 μg), $AP\text{-}EXO_{R\&L\&S}$ (DiR labeled AP-EXO (30 μg) incubated with RVG-CP05 (30 μg), ILP-CP05 (30 μg), ISP-CP05 (30 μg)) or Cy5.5 labeled RVG-CP05 were administered intravenously into C57BL/6 mice, or spinal cord injury mice model, respectively. Perfusion was performed 2 h after injection with 50 ml of cold PBS to wash out exosomes in circulation. Spinal cord, quadriceps, triceps, liver, spleen,

heart, lung, kidney and brain were harvested for imaging with IVIS spectrum (PerkinElmer) as per manufacturer's instructions. For the quantification of fluorescence intensity in each individual tissue, each tissue was encircled as the interested region and the fluorescence intensity was calculated automatically with the living image software (caliper life science, US). To test cellular uptake of exosomes *in vitro*, the spinal cord tissues were collected and fixed in 4% paraformaldehyde followed by dehydration with sucrose and embedded. Sections of 6 μm was cut and examined with rabbit *anti*-NF200 (1:200, Abcam, ab8135), mouse *anti*-GFAP (1:300, Cell Signaling technology, #3670) and goat *anti*-IbaI (1:200, Abcam, ab48004), polyclonal antibodies were detected by goat anti-rabbit IgG Alexa Fluor 488 (1:1000, Invitrogen), goat anti-mouse 555 (1:1000, Invitrogen), donkey anti-goat 647 (1:1000, Invitrogen). Colocalization of exosomes (DiR labeled) to different cell types were visualized by the whole landscape imaging system (PerkinElmer, Vectra Polaris, US). For detecting the sustain of AP-$EXO_{R\&L\&S}$ in the injured spinal cord, DiR labeled AP-EXO (30 μg), incubated with Alexa Fluor 405-labeled RVG-CP05 (30 μg), FAM-labeled ILP-CP05 (30 μg) and rhodamine-labeled ISP-CP05 (30 μg) were intravenously injected into the contused SCI mice for 2 h, 1 day, 3 days or 7days, spinal cord were dissected for imaging with IVIS spectrum followed by cutting into slices, and fluorescence of AP-EXO and the three peptides were imaged by Tissue FAXS Spectra (Austria), colocalization of the three peptides to AP-EXO were analyzed by Image J system.

4.9. Experimental design and administration

We designed a study to evaluate the effect of peptide-functionalized exosomes in the treatment of spinal cord injury *in vivo*. Animals in each group were specified in figure legends. For intravenous injections, exosomes from mouse plasma or human plasma were incubated with RVG-CP05 (EXO_{RVG}), ILP-CP05 (EXO_{ILP}) and ISP-CP05 (EXO_{ISP}) individually or together ($EXO_{R\&L\&S}$) were injected into tail veins of C57BL/6 or BALB/c nude mice at a dose of 1 mg/kg of exosomes (dissolves in 200 μl PBS, 1:1 ratio to exosomes and peptides), beginning at 24 h after injury and thereafter per week for 4 weeks.

4.10. Behavioral analysis

(1) Basso Mouse Scale (BMS)

To evaluate the recovery of hindlimb locomotory behavior in mice, BMS scores were performed before SCI, on day1, 7, and then weekly to 6 weeks after SCI according to guidelines of Basso Mouse Scale [30,52]. Mice were acclimated to the round open filed (1 m diameter) environment before testing. The round open field was surrounded by transparent glass plane for allowing observers to observe the hindlimb locomotory behavior of mouse. The experiments were carried out by two observers blinded to the experimental groups. Mice from different experimental groups were randomly tested and scored. Mouse was individually placed in the open filed and observed by two investigators for 4min. The scores of the BMS ranged from 0 to 9, with each score representing a different degree of hindlimb locomotory behavior. For example, no spontaneous movement of the hindlimb scored 0, while normal movement of hindlimb scored 9. The scores were based on multiple parameters of hindlimb movements such as joint movements, paw position, stepping pattern, coordination, trunk stability, and tail control.

(2) Catwalk gait analysis

The footprints, locomotory behavior and physical coordination of mice were objectively evaluated using the CatWalk XT system and CatWalk XT software (version 10.6, Noldus, Wageningen, the Netherlands) as previously described [53,54]. The CatWalk XT system consists of a walking platform with a transparent glass plate illuminated by a green LED light and a high-speed camera capturing the real footprints. The top of the walking platform is a ceiling with a red LED background, which visualizes the body contour of the mouse. The CatWalk testing was performed in a dark, quiet environment. Before testing, each mouse was trained to cross the illuminated glass walkway at least three times. The footprints of each mouse were recorded by the digital video camera blow the glass and were analyzed by the CatWalk XT software. Using this system, a series of parameters were recorded and analyzed including swing duration, base of support, stride length, stand, max contact area, swing speed. Swing duration: The swing duration is the time during which the paw is not in contact with the glass plate. Base of support: The base of support is measured by the perpendicular distance between the two hind-or front paws. Stride length: The stride length is the distance between the same paw travels during a step cycle. Stands: Duration of contact of a paw with the glass plate. Max contact area: Maximum area of a paw that comes into contact with the glass plate. Swing speed: Speed of the animal's paws in the recorded run.

4.11. Motor electrophysiology

Neural function was evaluated using an electrophysiological test after injury. The mice were deeply anesthetized with pentobarbital (30 mg/kg). The motor-evoked potentials (MEPs) of the mice were detected using electrophysiological devices (YRKJ-G2008; Zhuhai Yiruikeji Co., Ltd, Guangdong, China). A single 5-mA stimulation was administered to stimulate the motor region of the cerebral cortex.

4.12. Cortical spinal tract (CST) tracing

Mice were anesthetized with 4% isoflurane until unconscious followed by 2% isoflurane during surgery. Briefly, animals were head-fixed in a stereotaxic frame and a vertical midline incision was made from between the eyes to the posterior skull. With the bregma as the center in both the x and y planes, four microinjections point were precisely positioned (two injections/hemisphere, from bregma, anteroposterior (AP) coordination + 0.75 mm, mediolateral (ML) coordination ± 1.5 mm and AP – 0.5 mm, ML ± 1.0 mm) and burr holes were drilled over the sensorimotor cortex. Using a 10 μl Hamilton syringes with a 36 g beveled needle tip under control of digital stereotactic injector, 0.5 μl of 10% biotin dextran amine (BDA; MW 10000; Molecular Probes) was injected into one of the 4 total sites (Dorsoventral (DV) coordination: 0.5 mm from the cortical surface; rate: 0.1 μl/minute). After injection, the needle was kept in place for an additional 5 min to allow BDA diffusion and prevent backflow of the BDA to the surface, and then slowly withdrawn. Two weeks later, mice were anesthetized and perfused with 4% paraformaldehyde for detecting CST distribution in the spinal cord.

4.13. Perfusion and sectioning

Mice were deeply anesthetized, and the thoracic and abdominal cavity were opened along both costal margin under the xiphoid process. Pre-cooled PBS was first *trans*-cardially perfused, and when the outflow fluid from right atrial appendage became clear and the color of liver became pale, pre-cooled 4% paraformaldehyde was *trans*-cardially perfused. Spring scissors cut off bilateral lamina, the spinal cord is fully exposed. The spinal cord was harvested, kept straight, and fixed in 4% paraformaldehyde overnight at 4 °C. The tissue was dehydrated using a concentration gradient sucrose solution. The dehydrated spinal cords were frozen in OCT mounting media and sectioned on a cryotome (Leica, CM3050S, Germany) at a thickness of 6 μm or 25 μm (CST tracing). For series section staining of NF200 and GFAP, spinal cord specimens were picked up every 150 μm.

4.14. Immunohistochemistry and histology

Mounted sections were washed three times with PBS followed by blocking in 5% normal goat plasma (NGS) and 0.1% bovine plasma albumin (BSA) in PBS. 0.1% Triton X-100 was added to the blocking buffer depending on the antigen used. After blocking, sections were incubated in primary antibody diluted in blocking buffer overnight at 4 °C. Primary antibodies used were rabbit *anti*-NF200 (1:2000, Abcam, ab8135), *anti*-GFAP (1:200, Cell Signaling technology, #12389), *anti*-PSD95 (1:200, Cell Signaling technology, #3450), anti-5-HT (1:5000, Immunostar, 20080), goat *anti*-Iba1 (1:200, Abcam, ab48004), *anti*-PTPσ (1:50, R&D system, AF3430), *anti*-VGLUT1 (1:1000, Synaptic Systems, 135302), anti-CD31 (1:200, Abcam, ab222783), CD68 (1:500; Abcam, ab125212) and mouse *anti*-Synapsin 1 (1:200, Synaptic Systems, 106,011), *anti*-GFAP (1:300, Cell Signaling technology, #3670), anti-Choline Acetyltransferase (1:500, Millipore, #AB144P), anti-GAD67 (1:500, Millipore, MAB5406), *anti*-LAR (1:500, BD Biosciences, 610350), anti–CS–56 (1:200, Sigma-Aldrich, c8035) and Chicken anti-beta III Tubulin (1:1000, Abcam, ab41489). The next day, the sections were washed extensively with PBS and incubated in the appropriate secondary antibody conjugated to Alexa Fluor 488, 555 or 647 (1:500, Invitrogen) for 2 h at room temperature. BDA tract-tracing was visualized with Alexa Fluor 594 conjugated streptavidin (Invitrogen, S32356). After extensive washing, the sections were cover-slipped using anti-fade reagent (Origene, China, ZLI-9557) and examined and photographed using deconvolution fluorescence microscopy and confocal microscope (Zeiss). Tiled scans of individual whole sections were scanned, oriented and overlaid using scanning confocal laser microscope (Zeiss, LSM900, Germany). GFAP, BDA and 5-HT positive areas were quantified using Image J software, threshold analysis was used to eliminate all background from each section, leaving only the patterns of GFAP, BDA and 5-HT expression. Axons labeled by tract tracing using BDA or 5-HT were quantified using image J software as per manufactures' protocol.

To examine the presence of CD3 T lymphocytes and CD68 macrophages in tissues from treated mice or controls, mouse tissues were fixed in Bouin's solution (Sigma-Aldrich) and embedded with paraffin. CD3+T lymphocytes or $CD68^{+}$ macrophages were stained with rabbit–anti-mouse polyclonal antibodies CD3 (1:200; Abcam, ab16669) or CD68 (1:500; Abcam, ab125212) and detected by goat anti-rabbit secondary antibody. Routine H&E staining was used to examine the overall inured-spinal cord, liver and kidney morphology and assess the level of infiltrating mononuclear cells.

4.15. Plasma index measurement

Mouse blood was taken immediately before cervical dislocation and centrifuged at 1500 rpm for 3 min. Serum was separated and stored at −80 °C. Analysis of levels of serum ALP, ALT, AST, BUN, CREA and UA was performed by the clinical laboratory (Tianjin Metabolic Disease Hospital, Tianjin Medical University, Tianjin, China).

4.16. Statistics analysis

All data were reported as mean value ± SEM. Statistical differences between different treated groups were evaluated by Sigma Stat (Systat Software Inc., Chicago, IL, US). Both parametric and non-parametric analyses were applied as specified in figure legends. Sample size was determined by G*Power 3.1.7 (Power analysis and Sample size). Significance was determined based in $P < 0.05$. For animal studies, age-matched mice were used and randomly divided into different groups.

Author contribution

N.R., S.F. and H.K. conceived the project, designed the experiments. N.R., X.K. and W.L. analyzed the data and wrote the manuscript with input from all authors. S.F. and X.K. supervised the project and interpreted the results. N.R. designed and characterized enhanced exosomes, N.R. and M.W. performed cellular experiments. N.R., W.L., Z.Y. and Z.L. performed the animal experiments. C.L. performed the intravenous injection. R.Z. and J.Z. performed animal experiments and behavioral analysis. X.K. reviewed the data and provided critical recommendations for the manuscript. B.F., W·S., X.Y., Z.W., H.Z. and reviewed the data and provided advice. S.F. and N.R. provided financial support.

Ethics approval and consent to participate

Animal Experiments:

All the animal experiments were approved by the Ethics Committee of Shandong University (Jinan, Shandong, China; ECSBMSSDU2021-2-014). All the authors compliance with all relevant ethical regulations.

Human plasma obtained:

All the human experiments were approved by the Ethics Committee of Tianjin Medical University General Hospital, Tianjin, China; IRB2020-YX-011-01. All the authors compliance with all relevant ethical regulations.

Declaration of competing interest

The authors declare no conflict of interest. N.R., S.F. and H.K. conceived the project, designed the experiments. N.R., X.K. and W.L. analyzed the data and wrote the manuscript with input from all authors. S.F. and X.K. supervised the project and interpreted the results. N.R. designed and characterized enhanced exosomes, N.R. and M.W. performed cellular experiments. N.R., W.L., Z.Y. and Z.L. performed the animal experiments. C.L. performed the intravenous injection. R.Z. and J.Z. performed animal experiments and behavioral analysis. X.K. reviewed the data and provided critical recommendations for the manuscript. B.F., W·S., X.Y., Z.W., H.Z. and reviewed the data and provided advice. S.F. and N.R. provided financial support. All the authors approved the final version of the manuscript.

Acknowledgements

The authors acknowledge Dr. Haifang Yin (School of Medical Laboratory, Tianjin Medical University, Tianjin, China) for critical review of the manuscript. This work was supported by the National Key Research and Development Project of Stem Cell and Transformation Research (2019YFA0112100),China. National Natural Science Foundation of China (81930070), National Natural Science Foundation of China (82102560), the Natural Science Foundation of Shandong Province, China (ZR2021QH097), the No.69 General Fund of China Postdoctoral Science Foundation (2021M691936) and Talent project of Shandong University (22480082063100), China. We thank Translational Medicine Core Facility of Shandong University for consultation and instrument availability that supported this work.

Appendix A. Supplementary data

Supplementary data to this article can be found online at https://doi.org/10.1016/j.bioactmat.2022.07.002.

References

[1] T.H. Hutson, S. Di Giovanni, The translational landscape in spinal cord injury: focus on neuroplasticity and regeneration, Nat. Rev. Neurol. 15 (2019) 732–745, https://doi.org/10.1038/s41582-019-0280-3.

[2] B.T. Benevento, M.L. Sipski, Neurogenic bladder, neurogenic bowel, and sexual dysfunction in people with spinal cord injury, Phys. Ther. 82 (2002) 601–612.

[3] C.S. Ahuja, et al., Traumatic spinal cord injury, Nat. Rev. Dis. Prim. 3 (2017), 17018, https://doi.org/10.1038/nrdp.2017.18.

[4] B.Y. Fan, et al., Liproxstatin-1 is an effective inhibitor of oligodendrocyte ferroptosis induced by inhibition of glutathione peroxidase 4, Neural Regen Res 16 (2021) 561–566, https://doi.org/10.4103/1673-5374.293157.

[5] J. Li, et al., Modulation of the crosstalk between schwann cells and macrophages for nerve regeneration: a therapeutic strategy based on a multifunctional tetrahedral framework nucleic acids system, Adv Mater (2022), e2202513, https://doi.org/10.1002/adma.202202513.

[6] M. Zhou, et al., A DNA nanostructure-based neuroprotectant against neuronal apoptosis via inhibiting toll-like receptor 2 signaling pathway in acute ischemic stroke, ACS Nano (2021), https://doi.org/10.1021/acsnano.1c09626.

[7] T.M. O'Shea, J.E. Burda, M.V. Sofroniew, Cell biology of spinal cord injury and repair, J. Clin. Invest. 127 (2017) 3259–3270, https://doi.org/10.1172/JCI90608.

[8] J.M. Cregg, et al., Functional regeneration beyond the glial scar, Exp. Neurol. 253 (2014) 197–207, https://doi.org/10.1016/j.expneurol.2013.12.024.

[9] E.J. Bradbury, E.R. Burnside, Moving beyond the glial scar for spinal cord repair, Nat. Commun. 10 (2019) 3879, https://doi.org/10.1038/s41467-019-11707-7.

[10] Y. Shen, et al., PTPsigma is a receptor for chondroitin sulfate proteoglycan, an inhibitor of neural regeneration, Science 326 (2009) 592–596, https://doi.org/10.1126/science.1178310.

[11] B.T. Lang, et al., Modulation of the proteoglycan receptor PTPsigma promotes recovery after spinal cord injury, Nature 518 (2015) 404–408, https://doi.org/10.1038/nature13974.

[12] D. Fisher, et al., Leukocyte common antigen-related phosphatase is a functional receptor for chondroitin sulfate proteoglycan axon growth inhibitors, J. Neurosci. 31 (2011) 14051–14066, https://doi.org/10.1523/JNEUROSCI.1737-11.2011.

[13] G.C. Terstappen, A.H. Meyer, R.D. Bell, W. Zhang, Strategies for delivering therapeutics across the blood-brain barrier, Nat. Rev. Drug Discov. 20 (2021) 362–383, https://doi.org/10.1038/s41573-021-00139-y.

[14] G. van Niel, G. D'Angelo, G. Raposo, Shedding light on the cell biology of extracellular vesicles, Nat. Rev. Mol. Cell Biol. 19 (2018) 213–228, https://doi.org/10.1038/nrm.2017.125.

[15] S. Kamerkar, et al., Exosomes facilitate therapeutic targeting of oncogenic KRAS in pancreatic cancer, Nature 546 (2017) 498–503, https://doi.org/10.1038/nature22341.

[16] M. Nakazaki, T. Morita, K.L. Lankford, P.W. Askenase, J.D. Kocsis, Small extracellular vesicles released by infused mesenchymal stromal cells target M2 macrophages and promote TGF-beta upregulation, microvascular stabilization and functional recovery in a rodent model of severe spinal cord injury, J. Extracell. Vesicles 10 (2021), e12137, https://doi.org/10.1002/jev2.12137.

[17] L. Li, et al., Transplantation of human mesenchymal stem-cell-derived exosomes immobilized in an adhesive hydrogel for effective treatment of spinal cord injury, Nano Lett. 20 (2020) 4298–4305, https://doi.org/10.1021/acs.nanolett.0c00929.

[18] J.J. Li, et al., In vivo evidence for the contribution of peripheral circulating inflammatory exosomes to neuroinflammation, J. Neuroinflammation 15 (2018) 8, https://doi.org/10.1186/s12974-017-1038-8.

[19] I.M. Kur, et al., Neuronal activity triggers uptake of hematopoietic extracellular vesicles in vivo, PLoS Biol. 18 (2020), e3000643, https://doi.org/10.1371/journal.pbio.3000643.

[20] X. Gao, et al., Anchor peptide captures, targets, and loads exosomes of diverse origins for diagnostics and therapy, Sci. Transl. Med. 10 (2018), https://doi.org/10.1126/scitranslmed.aat0195.

[21] L. Cheng, et al., LAR inhibitory peptide promotes recovery of diaphragm function and multiple forms of respiratory neural circuit plasticity after cervical spinal cord injury, Neurobiol. Dis. 147 (2021), 105153, https://doi.org/10.1016/j.nbd.2020.105153.

[22] H. Wang, et al., Chondroitin-4-sulfation negatively regulates axonal guidance and growth, J. Cell Sci. 121 (2008) 3083–3091, https://doi.org/10.1242/jcs.032649.

[23] S. Gluska, et al., Rabies Virus Hijacks and accelerates the p75NTR retrograde axonal transport machinery, PLoS Pathog. 10 (2014), e1004348, https://doi.org/10.1371/journal.ppat.1004348.

[24] F. Luo, et al., Modulation of proteoglycan receptor PTPsigma enhances MMP-2 activity to promote recovery from multiple sclerosis, Nat. Commun. 9 (2018) 4126, https://doi.org/10.1038/s41467-018-06505-6.

[25] Y. Rong, et al., Neural stem cell small extracellular vesicle-based delivery of 14-3-3t reduces apoptosis and neuroinflammation following traumatic spinal cord injury by enhancing autophagy by targeting Beclin-1, Aging (Albany NY) 11 (2019) 7723–7745, https://doi.org/10.18632/aging.102283.

[26] Y. Rong, et al., Neural stem cell-derived small extracellular vesicles attenuate apoptosis and neuroinflammation after traumatic spinal cord injury by activating autophagy, Cell Death Dis. 10 (2019) 340, https://doi.org/10.1038/s41419-019-1571-8.

[27] C.S. Siegel, K.L. Fink, S.M. Strittmatter, W.B. Cafferty, Plasticity of intact rubral projections mediates spontaneous recovery of function after corticospinal tract injury, J. Neurosci. 35 (2015) 1443–1457, https://doi.org/10.1523/JNEUROSCI.3713-14.2015.

[28] A. Takeoka, I. Vollenweider, G. Courtine, S. Arber, Muscle spindle feedback directs locomotor recovery and circuit reorganization after spinal cord injury, Cell 159 (2014) 1626–1639, https://doi.org/10.1016/j.cell.2014.11.019.

[29] R. van den Brand, et al., Restoring voluntary control of locomotion after paralyzing spinal cord injury, Science 336 (2012) 1182–1185, https://doi.org/10.1126/science.1217416.

[30] D.M. Basso, et al., Basso Mouse Scale for locomotion detects differences in recovery after spinal cord injury in five common mouse strains, J. Neurotrauma 23 (2006) 635–659, https://doi.org/10.1089/neu.2006.23.635.

[31] J.K. Lee, et al., Assessing spinal axon regeneration and sprouting in Nogo-, MAG-, and OMgp-deficient mice, Neuron 66 (2010) 663–670, https://doi.org/10.1016/j.neuron.2010.05.002.

[32] J.R. Plemel, et al., A graded forceps crush spinal cord injury model in mice, J. Neurotrauma 25 (2008) 350–370, https://doi.org/10.1089/neu.2007.0426.

[33] L. Blanc, A. De Gassart, C. Geminard, P. Bette-Bobillo, M. Vidal, Exosome release by reticulocytes-an integral part of the red blood cell differentiation system, Blood Cells Mol. Dis. 35 (2005) 21–26, https://doi.org/10.1016/j.bcmd.2005.04.008.

[34] Q. Zhan, et al., Engineering blood exosomes for tumor-targeting efficient gene/chemo combination therapy, Theranostics 10 (2020) 7889–7905, https://doi.org/10.7150/thno.45028.

[35] A.C. Matei, L. Antounians, A. Zani, Extracellular vesicles as a potential therapy for neonatal conditions: state of the art and challenges in clinical translation, Pharmaceutics 11 (2019), https://doi.org/10.3390/pharmaceutics11080404.

[36] C. Yang, et al., Autologous exosome transfer: a new personalised treatment concept to prevent colitis in a murine model, J Crohns Colitis 14 (2020) 841–855, https://doi.org/10.1093/ecco-jcc/jjz184.

[37] S. Dai, et al., Phase I clinical trial of autologous ascites-derived exosomes combined with GM-CSF for colorectal cancer, Mol. Ther. 16 (2008) 782–790, https://doi.org/10.1038/mt.2008.1.

[38] G. Yu, H. Jung, Y.Y. Kang, H. Mok, Comparative evaluation of cell- and serum-derived exosomes to deliver immune stimulators to lymph nodes, Biomaterials 162 (2018) 71–81, https://doi.org/10.1016/j.biomaterials.2018.02.003.

[39] O. von Bohlen Und Halbach, V. von Bohlen Und Halbach, BDNF effects on dendritic spine morphology and hippocampal function, Cell Tissue Res. 373 (2018) 729–741, https://doi.org/10.1007/s00441-017-2782-x.

[40] N. Ran, et al., Effects of exosome-mediated delivery of myostatin propeptide on functional recovery of mdx mice, Biomaterials 236 (2020), 119826, https://doi.org/10.1016/j.biomaterials.2020.119826.

[41] Y.J. Li, et al., Gemcitabine loaded autologous exosomes for effective and safe chemotherapy of pancreatic cancer, Acta Biomater. 101 (2020) 519–530, https://doi.org/10.1016/j.actbio.2019.10.022.

[42] O.P. Wiklander, et al., Extracellular vesicle in vivo biodistribution is determined by cell source, route of administration and targeting, J. Extracell. Vesicles 4 (2015), 26316, https://doi.org/10.3402/jev.v4.26316.

[43] P. Kumar, et al., Transvascular delivery of small interfering RNA to the central nervous system, Nature 448 (2007) 39–43, https://doi.org/10.1038/nature05901.

[44] M. Lafon, Rabies virus receptors, J. Neurovirol. 11 (2005) 82–87, https://doi.org/10.1080/13550280590900427.

[45] Brommer, B. et al. Improving hindlimb locomotor function by Non-invasive AAV-mediated manipulations of propriospinal neurons in mice with complete spinal cord injury. Nat. Commun. 12, 781, doi:10.1038/s41467-021-20980-4.(2021).

[46] R.C. de Abreu, et al., Native and bioengineered extracellular vesicles for cardiovascular therapeutics, Nat. Rev. Cardiol. 17 (2020) 685–697, https://doi.org/10.1038/s41569-020-0389-5.

[47] M. Mathieu, L. Martin-Jaular, G. Lavieu, C. Thery, Specificities of secretion and uptake of exosomes and other extracellular vesicles for cell-to-cell communication, Nat. Cell Biol. 21 (2019) 9–17, https://doi.org/10.1038/s41556-018-0250-9.

[48] J. Regueiro, N. Olguin, J. Simal-Gandara, C. Sunol, Toxicity evaluation of new agricultural fungicides in primary cultured cortical neurons, Environ. Res. 140 (2015) 37–44, https://doi.org/10.1016/j.envres.2015.03.013.

[49] N. Olguin, M.L. Muller, E. Rodriguez-Farre, C. Sunol, Neurotransmitter amines and antioxidant agents in neuronal protection against methylmercury-induced cytotoxicity in primary cultures of mice cortical neurons, Neurotoxicology 69 (2018) 278–287, https://doi.org/10.1016/j.neuro.2018.07.020.

[50] C. Thery, S. Amigorena, G. Raposo, A. Clayton, Isolation and characterization of exosomes from cell culture supernatants and biological fluids, *Curr Protoc Cell Biol* **Chapter** 3 (2006), https://doi.org/10.1002/0471143030.cb0322s30. Unit 3 22.

[51] K. Liu, et al., PTEN deletion enhances the regenerative ability of adult corticospinal neurons, Nat. Neurosci. 13 (2010) 1075–1081, https://doi.org/10.1038/nn.2603.

[52] Y. Wang, et al., Remodeling of lumbar motor circuitry remote to a thoracic spinal cord injury promotes locomotor recovery, Elife 7 (2018), https://doi.org/10.7554/eLife.39016.

[53] J.C. Heinzel, et al., Evaluation of functional recovery in rats after median nerve resection and autograft repair using computerized gait analysis, Front. Neurosci. 14 (2020), 593545, https://doi.org/10.3389/fnins.2020.593545.

[54] T. Kameda, Y. Kaneuchi, M. Sekiguchi, S.I. Konno, Measurement of mechanical withdrawal thresholds and gait analysis using the CatWalk method in a nucleus pulposus-applied rodent model, J Exp Orthop 4 (2017) 31, https://doi.org/10.1186/s40634-017-0105-5.